



National Library
of Canada

Acquisitions and
Bibliographic Services Branch

395 Wellington Street
Ottawa, Ontario
K1A 0N4

Bibliothèque nationale
du Canada

Direction des acquisitions et
des services bibliographiques

395, rue Wellington
Ottawa (Ontario)
K1A 0N4

Your file *Votre référence*

Our file *Notre référence*

NOTICE

The quality of this microform is heavily dependent upon the quality of the original thesis submitted for microfilming. Every effort has been made to ensure the highest quality of reproduction possible.

If pages are missing, contact the university which granted the degree.

Some pages may have indistinct print especially if the original pages were typed with a poor typewriter ribbon or if the university sent us an inferior photocopy.

Reproduction in full or in part of this microform is governed by the Canadian Copyright Act, R.S.C. 1970, c. C-30, and subsequent amendments.

AVIS

La qualité de cette microforme dépend grandement de la qualité de la thèse soumise au microfilmage. Nous avons tout fait pour assurer une qualité supérieure de reproduction.

S'il manque des pages, veuillez communiquer avec l'université qui a conféré le grade.

La qualité d'impression de certaines pages peut laisser à désirer, surtout si les pages originales ont été dactylographiées à l'aide d'un ruban usé ou si l'université nous a fait parvenir une photocopie de qualité inférieure.

La reproduction, même partielle, de cette microforme est soumise à la Loi canadienne sur le droit d'auteur, SRC 1970, c. C-30, et ses amendements subséquents.

Field Adsorption, Desorption and Evaporation

by
Richard Liang-Chen Wang*

©Copyright by Richard L.C. Wang, 1992

Submitted in partial fulfillment
of the requirements for the degree of
Doctor of Philosophy
at
Dalhousie University
Halifax, Nova Scotia, Canada
June 9, 1992



National Library
of Canada

Acquisitions and
Bibliographic Services Branch

395 Wellington Street
Ottawa, Ontario
K1A 0N4

Bibliothèque nationale
du Canada

Direction des acquisitions et
des services bibliographiques

395, rue Wellington
Ottawa (Ontario)
K1A 0N4

Your file *Votre référence*

Our file *Notre référence*

The author has granted an irrevocable non-exclusive licence allowing the National Library of Canada to reproduce, loan, distribute or sell copies of his/her thesis by any means and in any form or format, making this thesis available to interested persons.

L'auteur a accordé une licence irrévocable et non exclusive permettant à la Bibliothèque nationale du Canada de reproduire, prêter, distribuer ou vendre des copies de sa thèse de quelque manière et sous quelque forme que ce soit pour mettre des exemplaires de cette thèse à la disposition des personnes intéressées.

The author retains ownership of the copyright in his/her thesis. Neither the thesis nor substantial extracts from it may be printed or otherwise reproduced without his/her permission.

L'auteur conserve la propriété du droit d'auteur qui protège sa thèse. Ni la thèse ni des extraits substantiels de celle-ci ne doivent être imprimés ou autrement reproduits sans son autorisation.

ISBN 0-315-80212-X

Canada

To my mother

CONTENTS

List of Figures	vii
List of Tables	viii
Abstract	ix
List of Symbols	x
Acknowledgements	xiv
PART I: FIELD ADSORPTION	2
1. Introduction	2
2. Theory	6
2.1 Equations	6
2.2 Electron Density	10
2.3 Imposition of External Electric Fields	12
3. Field Adsorption of Metal Atoms	13
3.1 Binding Energies and Energy Barriers	13
3.2 Charge Density and Electrostatic Field	19
3.3 Core States	23
3.4 Dipole Moment	27
3.5 Conclusions	28
4. Field Adsorption of Rare Gases	30
4.1 Free-Field Case	30
4.2 Sharp Resonances	31
4.3 Binding Distance and Desorption Energy	33
4.4 Electron Density Distribution	37
4.5 Comments on Classical Models	41

PART II: THERMAL FIELD-DESORPTION	47
1. Introduction	47
2. Adiabatic and Diabatic States	50
2.1 Hamiltonian	50
2.2 Adiabatic States	51
2.3 Diabatic States	54
2.4 Two-State System	55
3. Kinetics	62
3.1 Uncoupled States and Coupling Terms	62
3.2 Master Equation	64
4. Discussion	66
4.1 Ion Yield	66
4.2 Thermal Desorption of Helium	71
5. Conclusions	75
 PART III: FIELD EVAPORATION OF METALS	 77
1. Introduction	77
2. Method	80
2.1 Adiabatic and Diabatic States	80
2.2 Perturbative Approach	82
3. Results	89
4. Conclusions	97
References	99

List of Figures

Fig. 1.1	Potential energy for <i>Nb</i> on jellium	15
Fig. 1.2	The scale law of activation energies	18
Fig. 1.3	Electronic density shift for <i>Ti</i> and <i>Nb</i>	20
Fig. 1.4	External electrostatic potential for <i>Ti</i> and <i>Nb</i>	21
Fig. 1.5	External electrostatic field strength for <i>Ti</i> and <i>Nb</i>	24
Fig. 1.6	1s energy levels and estimated charge for field-adsorbed <i>Ti</i>	26
Fig. 1.7	Desorption energies and binding distances for <i>He</i>	34
Fig. 1.8	Desorption energies and binding distances for <i>Ne</i>	38
Fig. 1.9	Electronic density shift for <i>He</i>	40
Fig. 1.10	Electronic density shift for <i>Ne</i>	42
Fig. 2.1	Adiabatic and diabatic energy curves	57
Fig. 2.2	Adiabatic and diabatic energy curves for <i>He</i> field-adsorbed on <i>W</i>	61
Fig. 2.3	Flight time for <i>He</i> desorbed from <i>W</i>	73
Fig. 2.4	Adsorption distance, activation energy and prefactor for <i>He</i>	74

List of Tables

Table 1.1	Energy barriers for <i>Ti</i> and <i>Nb</i>	17
Table 1.2	Dipole moments and polarizabilities for <i>Ti</i> and <i>Nb</i>	29
Table 3.1	Field dependence of activation barriers and prefactors for <i>W</i> evaporation	93

ABSTRACT

Using the density-functional theory with the local density approximation for the field adsorption of transition metal atoms, titanium and niobium, we obtain the electric field distribution and, especially, the field enhancement above an adsorbed metal atom. From detailed analyses of electron distributions of the rare-gas atoms, helium and neon, field-adsorbed on metals, we demonstrate that the increase in binding energies to several hundred meV with increasing field strengths can be attributed to a transition from physisorption in weak fields to field-induced chemisorption in strong fields.

We construct diabatic states from adiabatic ones by using a unitary transformation for the thermal field-desorption of helium from tungsten and developing a perturbational method for the field-evaporation of tungsten, respectively. The diabatic states form the basis to compute the temperature-dependent ionization probabilities for singly-charged ions. Employing a master equation, we calculate the energy-dependent ion yield as a function of field strength and temperature, and extract the field dependence of the activation barrier and prefactor.

List of Symbols

A	unitary transformation matrix
a_{iv}	annihilation operator of diabatic states
a_{iv}^+	creation operator of diabatic states
ASED-MO	Atom Superposition and Electron Delocalization Molecular Orbital method
b_J	annihilation operator of a phonon of mode J
b_J^+	creation operator of a phonon of mode J
E_{ad}	energy of an adatom
E_b	binding energy
E_{es}	total electrostatic energy of the system
E_F	Fermi energy
E_i	single-electron energy
E_t	total energy of a system
F	applied electric field strength
F_0	asymptotic electric field strength
F_{ev}	evaporation field strength
$G^M(r, r')$	outgoing-wave Green's function for a bare metal surface
h	single electron Hamiltonian
H	total Hamiltonian
H_A	Hamiltonian of the system of adatom-electrons (both in adatom and the metal)
H_e	Hamiltonian of the electrons
H_s	Hamiltonian of phonons
H'	interaction Hamiltonian

I_n	the n -th ionization potential of a desorbing ion
k	wavevector of continuum states
n^A	electron density of an isolated atom
$n(r)$	electron number density
n_i	occupation of the i -th orthonormal orbital
$n_i(t)$	occupation probability of diabatic states
$n^{MA}(r)$	electron number density of the metal-adatom system
$n^M(r)$	electron number density of the bare metal
$n^{(ph)}$	Bose-Einstein occupation function for phonons
N_a	normalization constant
P_n	projection operator
$Q(F)$	field dependent activation barrier
r_d	rate constant of a thermally activated process
r_s	Wigner-Seitz radius
R	position of an adatom nucleus
$R_i(\nu, \mu)$	phonon transition rate
S	overlap of electron orbitals
S	sticking coefficient
$T_{ij}(\nu, \mu)$	tunneling rate
T_N	kinetic energy operator of an adatom nucleus
u_j	normal phonon mode
$v_{es}(r)$	electrostatic potential for electrons
$v_{eff}[n; r]$	effective potential for electrons
$v_{xc}[n; r]$	exchange-correlation potential
V_k	interaction between levels ϕ_a and $\phi_{m,k}$
V_{vdW}	dispersion or van der Waals energy

W	diabatic interaction matrix
Y_{ion}	yield of singly charged ions
z_d	position of the dynamic image plane
Z	nuclear charge of an adatom
α	accommodation coefficient
α	polarisability
λ	rate constant
Λ	field-free sublimation (cohesive) energy of a metal
Γ	half-width
$\delta n(r, E)$	difference in electron number densities of a metal-adatom system and bare metal
$\delta n(E)$	difference in the densities of electron states
σ_0	area density of bare-metal electron
μ	dipole moment
ϵ	dielectric function of the solid
$\epsilon_c(n)$	correlation part of ϵ_{xc}
$\epsilon_{xc}(n)$	exchange-correlation energy per particle of a uniform electron gas of density n
ν	vibrational frequency around the minimum
ζ_i	adiabatic many electron wavefunctions
ξ_i	diabatic many electron wavefunctions
ϕ_a	the highest occupied single electron level with energy ϵ_a in the isolated adatom
ϕ_m	the lowest unoccupied level with energy ϵ_m above the Fermi energy of isolated metals

Φ	work function of the surface
Φ_g	molecular orbital with a lower energy ϵ_g
Φ_e	molecular orbital with a higher energy ϵ_e
$\Psi(R, t)$	field operator
$\psi_i(r)$	single electron wavefunction
$\psi^{MA}(r)$	wavefunction of the metal-adatom system
$\psi^M(r)$	wavefunction of bare metal
Ψ_α	wavefunction of Hamiltonian H_d
$\chi_{i\alpha}(R)$	adiabatic state of an adatom nucleus
η	diabatic state of an adatom nucleus

Acknowledgements

I express heartfelt thanks to Dr. H.J. Kreuzer for that he, and the Department of Physics, gives me the opportunity to complete a Ph.D. degree program in Physics, which has been my dream for about twenty years. I have benefitted very much from his marvellous intuition and his comprehensive and profound understanding of both theory and experiment at both microscopic and macroscopic levels.

I am also grateful to Dr. N.D. Lang for generously providing computer programmes and for helpful discussions.

Lastly, my deepest appreciation is given to my mother for her sacrifice, support and encouragement. My greatest regret is that she cannot share in person in my achievement. However, I feel her blessing from heaven. Thank you Mother.

The work presented in this thesis has been financially supported by the Natural Sciences and Engineering Research Council of Canada and the Office of Naval Research of United States of America.

In electrostatic fields of the order of volts per angstrom, as they occur in the vicinity of field ion tips, the physics and chemistry of atoms, molecules and metal surfaces exhibit rich novel features the most striking of which are field-induced adsorption of rare gases, field-induced chemical reactions of adsorbed molecules, field desorption and field ionization, the latter being the mechanism of image formation in the field ion microscope. Some recent reviews are listed in Refs.1-4. In this thesis, we focus on field adsorption, field desorption and field evaporation⁵⁻⁸.

PART I: FIELD ADSORPTION

1. Introduction

Electric fields of the order of volts per angstrom are comparable to those experienced by valence electrons in atoms and molecules. Thus one expects that, in external fields of that magnitude, a redistribution of the valence electrons in a coupled adsorbate-solid system takes place which affects the orbitals of both surface bonds and internal bonds in adsorbed molecules. Whether this redistribution leads to either enhanced or reduced binding depends on whether the bonding or antibonding orbitals are more strongly affected. We will refer to this phenomenon as field-induced chemisorption.

Surprisingly, field-induced chemisorption is important even for the most inert atom, namely helium. We recall that, in field-free cases, chemisorption is rather unimportant for the lighter rare gases because for them physisorption, arising from mutually induced fluctuating dipole-dipole interactions of the van der Waals type, dominates. In fields of the order of $5V/\text{\AA}$, polarization induces the occupation of excited states at the level of a few percent. Thus, in such fields, even helium cannot be regarded as a closed-shell atom, as it forms weak covalent bonds upon approach of a metal surface.

The first quantum mechanical calculation of the self-consistent charge density and electric field distribution at a metal surface was performed by Lang and Kohn⁹ for the case of a structureless jellium surface, using the local-density approximation to density-functional theory. Recently this problem was studied by Gies and Gerhardt,¹⁰ and also by Schreier and Rebentrost¹¹. Including the effect of the crystal structure, Inglesfield has performed self-consistent field calculations of *Al* and *Ag* surfaces^{12,13}. An early microscopic calculation of field-induced chemisorption by Kahn and Ying¹⁴ was also based on the local-density approximation of the density-functional formalism; they calculated the potential energy curves, and thus the activation energy, for alkali atoms on *W*, which they treated within the jellium model. Kingham¹⁵ has presented some preliminary results for the field evaporation of *Rh* obtained within a tight-binding cluster model with field effects and charge transfer treated in an ad hoc manner. Kreuzer *et al.*¹⁶⁻¹⁸ have recently presented a microscopic theory of field adsorption, in which the total energy of an adsorbing atom or molecule, in interaction with a metal and subjected to a self-consistently determined external electric field, is calculated by using a tight-binding approach based on the ASED-MO¹⁹ method.

Imaging of single atoms in the field ion microscope is believed to result from local field enhancement around kink sites and step edge sites on flat crystal planes. These local electric fields, of the order of $V/\text{\AA}$, arise, via Poisson's equation, from locally

enhanced surface charge density. To understand this phenomenon on a microscopic level, it is mandatory to calculate self-consistently the electronic charge distribution and the resulting electrostatic field at kink sites or around single atoms on densely packed planes of transition metals. As a model of the latter, we will present self-consistent calculations of the electric field around a metal atom adsorbed on a structureless jellium surface, using local-density-functional theory. As examples, we consider a light and a moderately heavy metal atom, *Ti* and *Nb*, respectively, on a jellium metal with a Wigner-Seitz radius $r_s = (3/4\pi n)^{1/3} = 3.0 \text{ bohr}$, where n is the bulk electron density. We will restrict our consideration to the polarity in which the field points away from the surface, appropriate for the field ion microscope. Although our model describes the chemisorption of metal atoms on a free electron metal in the presence of a field, we will see below that the results have quite general features that allow a discussion of field effects in chemisorption on transition metals. With the numerical results of the adsorption of *Ti* and *Nb* atoms on jellium metal surface in the presence of external electric fields, we will recover the field enhancement. We will also produce the adsorption potential well for these atoms and calculate the evaporation field strength, above which surface atoms are no longer bound to the surface. Despite the simplicity of the jellium model, we find very good agreement with both experimental values and earlier semi-empirical calculations, based on the ASED-MO method^{1,20}. We will also discuss the dipole moment and polarizability of the adsorbed atom to make a connection with some experi-

mental results.

Rare-gase atoms adsorb on metals with typical binding energies of 6meV for helium, 35meV for neon, 70meV for argon and 250meV for xenon. In static electric fields of the order of several $V/\text{\AA}$, the adsorption energy of helium and neon increase by at least an order of magnitude, leading to field adsorption of rare-gase atoms at elevated temperatures on top of edge and kink atoms, where the local field is greatly enhanced, as already deduced from early atom probe results²¹⁻²³. Recent measurements yield values of the order of 200meV for helium and 300meV for neon in a field of $4.5V/\text{\AA}$ ^{18,24}. The interaction between rare-gas atoms and metals in the presence of high external electric field, which is known as field-induced adsorption, plays an important role in the imaging process of the Field Ion Microscope. To explain this phenomenon, Tsong and Müller^{23,25} proposed a classical dipole-dipole interaction model, in which a polarized *He* atom is attracted by the polarized *W* atoms on the surface. However, Kreuzer *et al.*^{16-18,26} demonstrated that field-induced adsorption was not governed by the van der Waals and field-induced dipole-dipole interaction, but by field-induced weak chemisorption accompanied by a significant reduction of the binding distance. In this thesis, with a fully self-consistent calculation, we demonstrate how the field-induced adsorption of rare-gas atoms on metal surfaces transfers from physisorption to weak chemisorption with increasing strength of the external electric field. The essential point is that the external electric field raises the energy levels of the valence

electrons of the rare-gas atoms up to the energy band of the valence electrons of the metal, and it leads to strengthen interactions and, therefore, shorten binding distances.

In the next section we collect the relevant equations and specify the boundary conditions. In subsequent sections, we discuss adsorption of metal atoms, *Ti* and *Nb*, and rare-gas atoms, *He* and *Ne*, respectively, on jellium metal surface in the presence of an external electric field.

2. Theory

2.1 Equations

In the classical electromagnetic theory, the surface of a metal is represented as a mathematical plane with excess charges and a dipole layer, at which the normal component of the electric field drops discontinuously to zero, at least for a perfect conductor. On real surfaces, however, the electron distribution and electric fields vary smoothly over distances of a few angstroms. A simple model^{9,27}, which exhibits these features, is the jellium model of a metal, in which it is assumed that the ionic lattice smears into a uniform positive-charge density, n_+ , that drops abruptly to zero half a lattice constant above the topmost layer of ion cores. In front of this jellium metal, we add a metal atom²⁸, around which we will study the local electron and field distribution within the framework of density-functional theory.

The formalism of Kohn and Sham²⁹ reduces the many-body problem of the ground-state density distribution, $n(\mathbf{r})$, of an inhomogeneous system of N electrons in an electrostatic potential $v_{es}(\mathbf{r})$ to the self-consistent solution of the equations (we use Rydberg units, with $|e| = 2m = \hbar = 1$)

$$(-\nabla^2 + v_{eff}[n;\mathbf{r}]) \psi_i(\mathbf{r}) = E_i \psi_i(\mathbf{r}), \quad (1.1)$$

with

$$n(\mathbf{r}) = \sum_i n_i |\psi_i(\mathbf{r})|^2, \quad (1.2)$$

where n_i indicates the occupation of the i th orthonormal orbital. The effective potential in Eq.(1.1) is given by

$$v_{eff}[n;\mathbf{r}] = v_{es}(\mathbf{r}) + v_{xc}[n;\mathbf{r}]. \quad (1.3)$$

In Eq.(1.3) $v_{es}(\mathbf{r})$ is the electrostatic potential seen by an electron, due here to the adatom nucleus, positive background and electronic charge distribution. It is determined from Poisson's equation

$$\nabla^2 v_{es}(\mathbf{r}) = 2 \times 4\pi e [n_+ \theta(-z) + Z\delta(\mathbf{r}-\mathbf{R}) - n(\mathbf{r})], \quad (1.4)$$

where $z=0$ is chosen as the jellium edge and the semi-infinite space, $z < 0$, is occupied by the jellium, $\theta(x)$ is the Heaviside step

function, defined as 1 if $x \geq 0$ and 0 if $x < 0$, and R is the position of the adatom nucleus. The other term in Eq.(1.3), $v_{xc}[n;r]$, is the exchange-correlation potential, the local-density approximation²⁹ to which is

$$v_{xc}(n(r)) = \left. \frac{dn\epsilon_{xc}(n)}{dn} \right|_{n=n(r)}$$

$$= -2 \left[\frac{3}{\pi} n(r) \right]^{1/3} + \left. \frac{dn\epsilon_c(n)}{dn} \right|_{n=n(r)} . \quad (1.5)$$

The factors of 2 appearing in Eqs.(1.4) and (1.5) result from the use of Rydberg unit system. In Eq.(1.5), $\epsilon_{xc}(n)$ is the exchange-correlation energy per particle of a uniform electron gas of density n and $\epsilon_c(n)$ is its correlation part. The expression of $\epsilon_c(n)$ used here is that given by Hedin and Lundqvist³⁰.

Let us denote the electron number density of the metal-adatom system by $n^{MA}(r)$ and the corresponding electron number density of the bare metal by $n^M(r)$. The wavefunction of the metal-adatom system, $\psi^{MA}(r)$, and that of the bare metal, $\psi^M(r)$, specified by a continuum energy eigenvalue E and other quantum numbers, Q , which being omitted here for now, satisfy the differential equations

$$(\nabla^2 + E - v_{eff}[n^M;r]) \psi^M(r) = 0 \quad (1.6a)$$

and

$$(\nabla^2 + E - v_{eff}[n^{MA}; r]) \psi^{MA}(r) = 0, \quad (1.6b)$$

respectively. The latter can be rewritten in the following form,

$$(\nabla^2 + E - v_{eff}[n^M; r]) \psi^{MA}(r) = \delta v_{eff}(r) \psi^{MA}(r), \quad (1.7)$$

where

$$\delta v_{eff}(r) = v_{eff}[n^{MA}; r] - v_{eff}[n^M; r]. \quad (1.8)$$

Eq.(1.7) is equivalent to the Lippmann-Schwinger equation,

$$\psi^{MA}(r) = \psi^M(r) + \int G^M(r, r') \delta v_{eff}(r') \psi^{MA}(r') dr', \quad (1.9)$$

where the outgoing-wave Green's function for the bare-metal surface, $G^M(r, r')$, specified by the same continuum energy E and other quantum numbers Q as those for the wavefunction $\psi^M(r)$, is defined by the equation

$$(\nabla^2 + E - v_{eff}[n^M; r]) G^M(r, r') = \delta(r-r'). \quad (1.10)$$

Because $\delta v_{eff}(r)$ approaches zero rapidly outside the adatom, one can restrict the integral in (1.9) to a sphere centered at the adatom and bounded by a surface S , outside of which δv_{eff} is negligible.

The total energy of the system becomes

$$E_t = \sum_i E_i n_i + E_{es} - \int v_{eff}[n;r] n(r) dr + \int \epsilon_{xc}(n(r)) n(r) dr, \quad (1.11)$$

where E_{es} is the total electrostatic energy of the system. As the metal-adatom system is an infinite system, the theory actually calculates the total energy difference between the metal-adatom system and bare metal as a function of the adatom's position, R , and the field strength, F_0 ,

$$E_{ad}(R, F_0) = E_t^{MA}(R, F_0) - E_t^M(F_0), \quad (1.12)$$

which is termed as the energy of the adatom.

2.2 Electron Density

Having the (normalized) wavefunction of the bare metal, $\psi_{EQ}^M(r)$, belonging to the continuum energy E and other quantum numbers Q , the wavefunction of the metal-adatom system, $\psi_{EQ}^{MA}(r)$, is obtained by integrating the Lippmann-Schwinger equation (1.9). It belongs to the same continuum energy E and quantum numbers Q as those for $\psi_{EQ}^M(r)$, and it will also have the same normalization as the $\psi_{EQ}^M(r)$, a fact which facilitates the calculation of the electron density distribution and the state density. Then, we can express the difference of the electron number density between the metal-

adatom system and bare metal, $\delta n(r, E)$, as a function of the space coordinate r and energy E , as a summation (or integration) over Q ,

$$\begin{aligned} \delta n(r, E) = & 2 \sum_Q \theta(E - E_0) [|\psi_{EQ}^{MA}(r)|^2 - |\psi_{EQ}^M(r)|^2] \\ & + 2 \sum_{Qc} \delta(E - E_c) |\psi_{EcQc}^{MA}(r)|^2, \end{aligned} \quad (1.13)$$

where $E_0 \equiv v_{eff}(-\infty)$ is the value of v_{eff} deep in the metal, i.e., the bottom of the metal band, and $\psi_{EcQc}^{MA}(r)$ is the discrete state of the adsorbed atom with the energy eigenvalue E_c and additional quantum numbers Q_c . The factor of 2 accounts for spin degeneracy as we use a spin-unpolarized formalism. The difference in electron density between the metal-adatom system and bare metal is

$$\delta n(r) = n^{MA}(r) - n^M(r) = \int_{-\infty}^{E_F} \delta n(r, E) dE, \quad (1.14)$$

where $E_F = E_0 + k_F^2$ is the Fermi energy with k_F being defined in terms of the Wigner-Seitz radius r_s , $k_F \equiv (9\pi/4)^{1/3} / r_s$. The electron density in the metal-adatom system, $n^{MA}(r)$, is calculated as the sum, $n^M(r) + \delta n(r)$, with $n^M(r)$ evaluated directly in the semi-infinite bare-metal case⁹. The electron density, $n^{MA}(r)$, is then used to re-evaluate v_{eff} from Eq.(1.3); and a self-consistent electron density is obtained by iteration.

Integrating the function $\delta n(r, E)$ over the space coordinate, we obtain the difference in the density of electron state defined as

$$\delta n(E) = \int \delta n(r, E) dr. \quad (1.15)$$

2.3 Imposition of External Electric Fields

To include an external electric field into the model, one must add an excess surface charge to the metal. This is done first in the bare metal problem by imposing the following condition,

$$\sigma_0 = e \int_{-\infty}^{\infty} (n_{+0}(-z) - n^M(z, F_0)) dz = \frac{F_0}{4\pi}, \quad (1.16)$$

on the electron density of the bare metal, leading to wavefunctions $\psi^M(r, F_0)$ and electron densities $n^M(r, F_0)$, that depend explicitly on the asymptotic field strength, F_0 , far from the surface. In the presence of an adatom, one requires that outside the sphere S

$$n^{MA}(r; F_0) \rightarrow n^M(r; F_0), \quad \text{for } |r| \rightarrow \infty. \quad (1.17)$$

This imposes a boundary condition on the solution of (1.9), thereby incorporating the effect of the external electric field on the metal-adatom system.

While the external electric field does not change the structure of the one-electron equations, it does affect the numerical procedure. In the absence of such external electric fields, the effective potential of a bare metal, $v_{eff}[n^M; z]$, approaches a constant for $z \rightarrow \infty$, which is usually taken as the energy reference. However, in the presence of an external electric field with asymptotic strength F_0 , $v_{eff}[n^M; z]$ grows as eF_0z for large z . It is then advantageous to choose the value of the effective potential at the position of the adatom nucleus, $v_{eff}[n^{MS}; Z]$, as the energy reference. With this choice the energies of all occupied levels are negative.

A complication, arising in the presence of an electric field, is the fact that the potential-energy barrier of field adsorption varies from several eV , i.e., the cohesive energy in the absence of the field, down to zero at the evaporation field strength. Recalling that the theory calculates the energy difference, δE , between the metal-adatom system and the bare metal or the total energy of the adatom of the order of $10^4 eV$ for *Ti* and *Nb*, we need a relative precision for the total energy difference as high as the order of about 10^{-6} , a difficult task on numerics.

3. Field Adsorption of Metal Atoms

3.1 Binding Energies and Energy Barriers

We now present numerical results for two systems, titanium and

niobium, respectively, on a jellium metal surface with $r_s=3.0$ bohr.

In Fig.1.1, we show the adiabatic potential energy curves, the difference between the adatom's energy and the energy of an isolated atom in the field free case, i.e., $E_{ad}(Z, F_0) - E_{ad}(\infty, F_0=0)$, for a niobium atom adsorbed on a jellium for several field strengths as a function of the distance, Z , from the surface. In free field case, the depth of the potential energy curve is 5.2eV, which is, not surprisingly, somewhat less than the cohesive energy of Nb, 7.47eV, because the jellium lacks p - and d -orbitals. This deficiency is also the cause of the rather weak repulsion at short distances. As we apply a field, we note a shift of the potential minimum by about 0.2 \AA away from the surface, which can be traced to a transfer of electronic charge from outside the adatom to the region between the adatom and the surface. With an applied field, the ground-state energy curves will approach to their asymptotic form $-eF_0z$ for large z , appropriate to a singly charged positive ion. Ionization of the adatom can occur when its highest occupied level is lifted by the field energy term, eF_0z , above the Fermi level of the jellium. If the ionization level were not shifted and broadened by the interaction with the metal, the transition to the asymptotic form would happen abruptly at the apex of the potential energy curve, i.e., at the point where the diabatic energy curves for the neutral and singly-charged ionic species cross. For the fields chosen for Fig.1.1, the apex is so close to the metal surface that considerable interaction between the adatom and the metal is still in effect. This results in a considerable

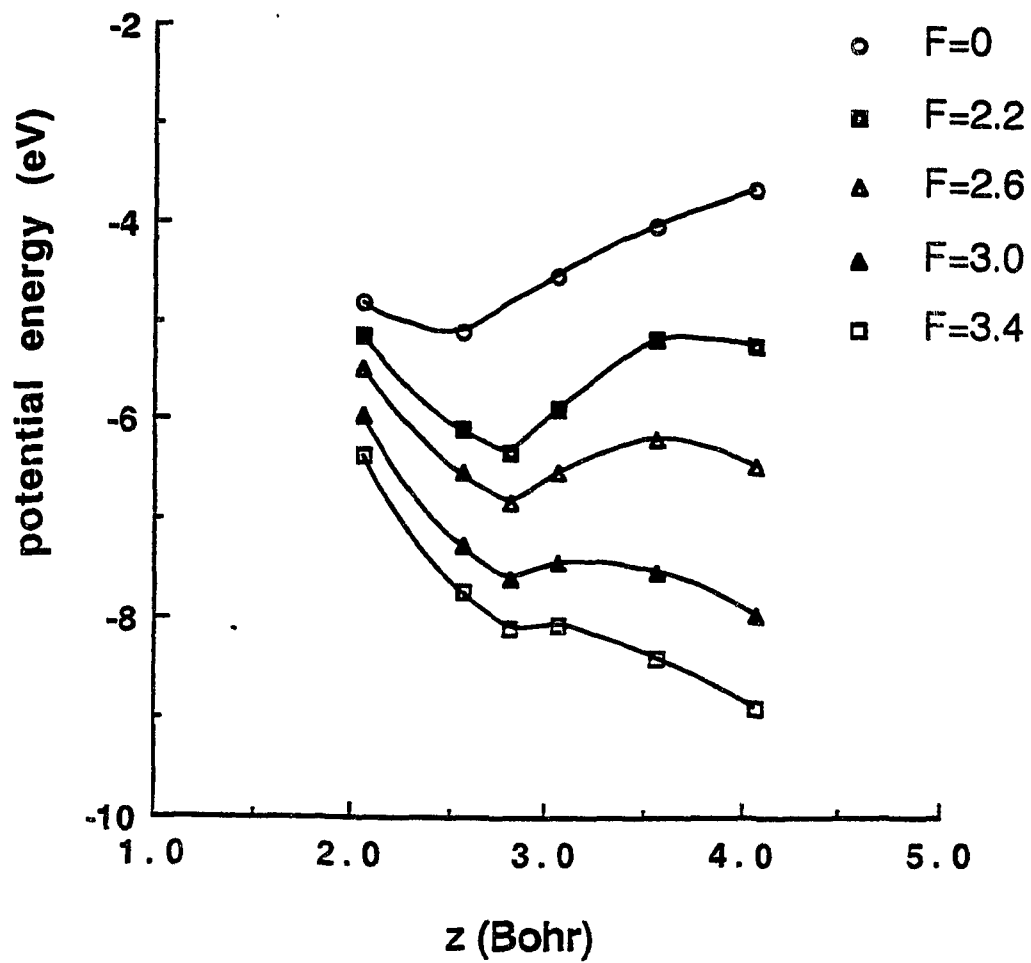


Fig.1.1: Potential energy for *Nb* on jellium with $r_s=3.0$ bohr as a function of nuclear distance, Z , from the jellium edge. F_0 in $V/\text{\AA}$.

broadening of the ionization level of the adatom, so that only partial charge-draining occurs in the apex region.

We will call the energy difference between the minimum at the adsorption equilibrium distance of the surface potential and the local maximum at its apex the activation energy, $Q(F_0)$, for ionization. In the field free case, the activation energy is equal to the binding energy of the adatom. The field strength, at which the activation energy becomes zero, is called the evaporation field strength, F_{ev} . We estimate the evaporation field strength for Nb adsorbed on jellium to be $3.6V/\text{\AA}$, which compares very favorably with the experimental value of the evaporation field strength for Nb , $3.5V/\text{\AA}$. Similar results are obtained for Ti . Binding energies and activation energies are collected in Table 1.1.

It has been suggested²⁰ that, if one plots $Q(F_0)/Q(F_0=0)$ as a function of $f=F_0/F_{ev}$, the field dependence of the activation energy for different metals obeys a universal scaling law. In a simple model, this scaling law is given by

$$\frac{Q(F_0)}{Q(F_0=0)} = \sqrt{1-f} + \frac{1}{2}f \ln \frac{1-\sqrt{1-f}}{1+\sqrt{1-f}}. \quad (1.18)$$

Experimental data on tungsten³² and theoretical results, obtained by the ASED-MO method²⁰, have confirmed this conjecture, as do the present results for Ti and Nb , shown in Fig.1.2.

Table 1.1: Energy barriers $Q(F_0)$ (in eV). The free field value, $Q(0)$, is the binding energy.

adatom	$F (V/\text{\AA})$				
	0.0	2.2	2.6	3.0	3.4
<i>Ti</i>	4.30	0.57	0.25	0.09	-
<i>Nb</i>	5.20	1.30	0.64	0.20	0.05

Experimental results³¹:

binding energy	4.85 eV for <i>Ti</i> and 7.47 eV for <i>Nb</i>
evaporation field	2.5 V/\AA for <i>Ti</i> and 3.5 V/\AA for <i>Nb</i>

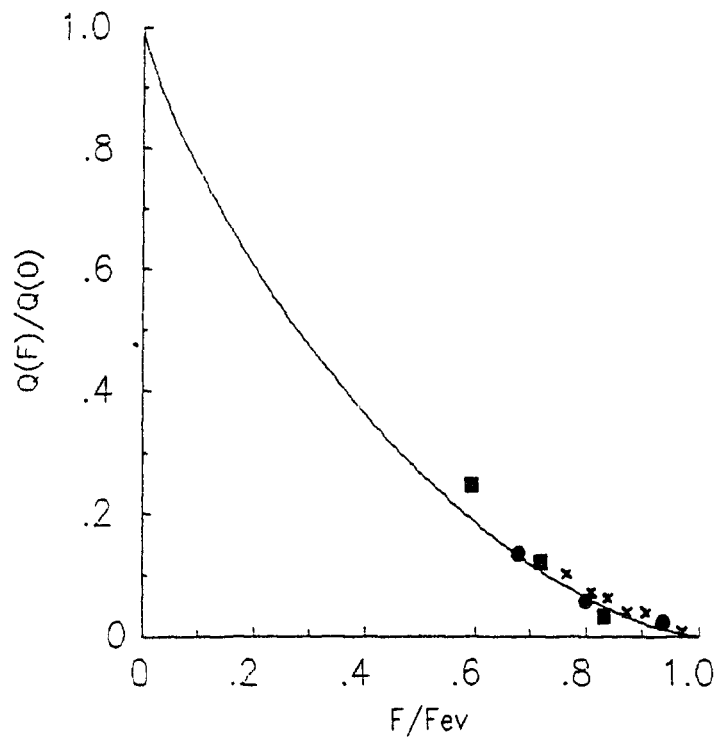


Fig.1.2: The activation energy, $Q(F)$, for field evaporation, normalized with the cohesive energy, $Q(0)=E_b$, as a function of asymptotic field strength F , normalized with the evaporation field strength, F_{ev} . Line are from Eq.(1.18) and crosses are experimental data for W from Ref.32. Our calculation results: black squares for Nb and black circles for Ti.

3.2 Charge Density and Electrostatic Field

In Fig.1.3, we show the electronic density shift,

$$\delta n(r, F_0) = n^{MA}(r, F_0) - n^M(r, F_0) - n^A(r, F_0), \quad (1.19)$$

due to the applied field, demonstrating an overall charge transfer from the region outside the adsorbed atom into the region between the adatom and the bulk and further into the bulk. From Poisson's equation for the electronic charge density difference $n^{MA}(r, F_0) - n^{MA}(r, F_0=0)$, we can calculate the total external electrostatic potential, which equals the sum of the applied external electrostatic potential and the electrostatic potential of the induced electron charge density, as the electrostatic potential difference in the presence and absence of an excess charge density, $\sigma_0 = F_0/4\pi$, far from the adatom on the surface,

$$V_{ext}(r) = V_{es}(r, F_0) - V_{es}(r, F_0=0). \quad (1.20)$$

Equipotential contours are plotted in Fig.1.4 for *Ti* and *Nb*. The expulsion of the external field from the region of the metallic adatom is beautifully demonstrated, the effect being larger for the heavier *Nb* atom than for the lighter *Ti* atom.

Classical electrostatic theory predicts that the electrostatic potential around a hemispherical protrusion of radius R on an otherwise flat and structureless metal surface is given by³³

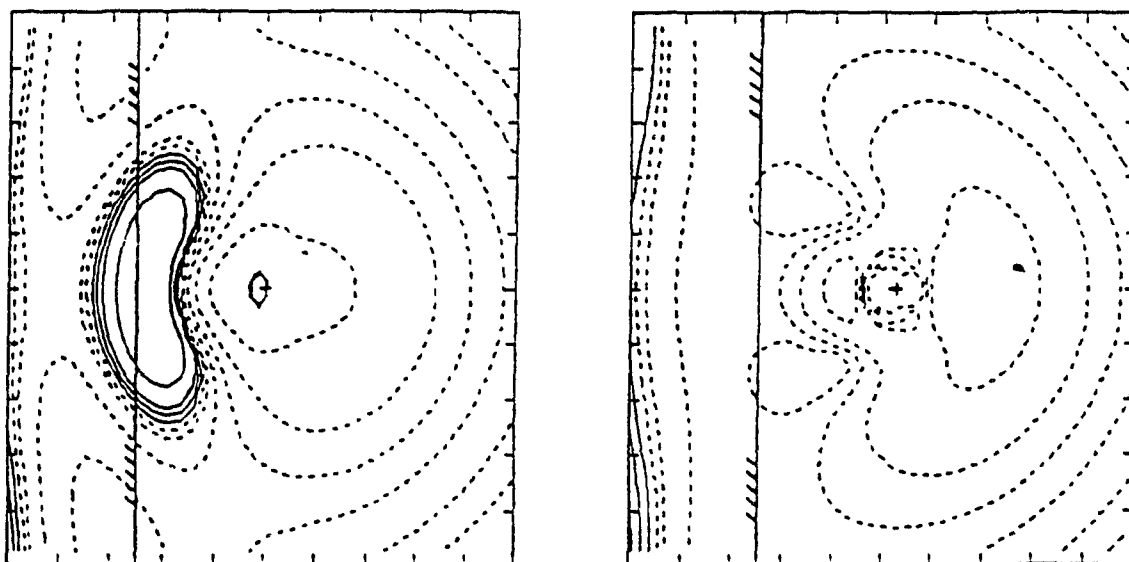


Fig.1.3: Electronic density shift in an electric field for the adatom at the minimum, d , of the potential energy. Left: Ti ($r_s=3.0\text{bohr}$ at $d=2.5\text{bohr}$) in $F_0=2.6\text{V/\AA}$. Right: Nb ($r_s=3.0\text{bohr}$ at $d=2.75\text{bohr}$) in $F_0=3.0\text{V/\AA}$. Contours $\delta n = 0, \pm 0.0001, \pm 0.002, \pm 0.005, \pm 0.001, \pm 0.002, \pm 0.005$ a.u. Solid (broken) lines non-negative (negative) values. Contours in the core region are omitted.

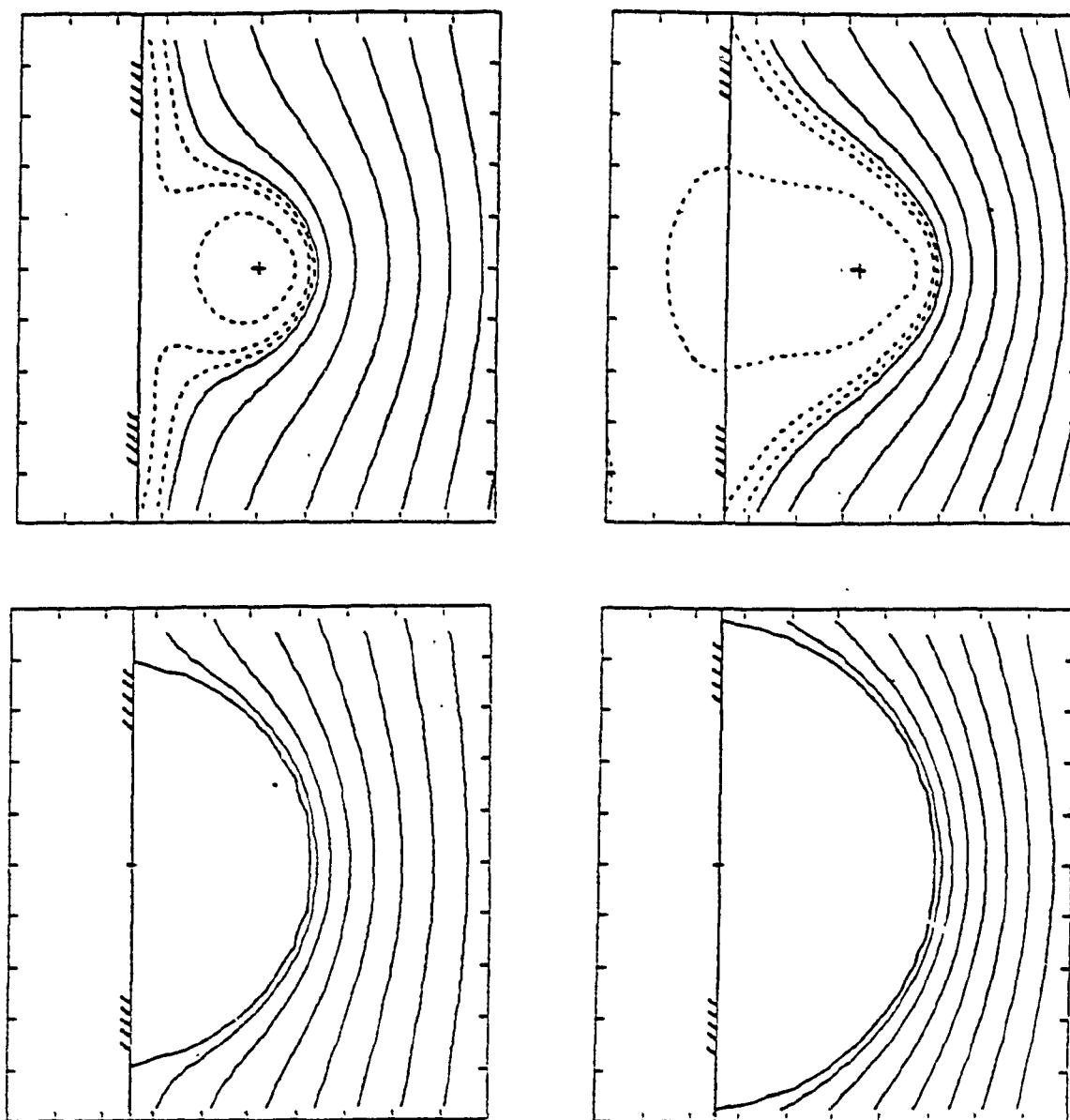


Fig.1.4: External electrostatic potential, upper panels for the same systems as Fig.1.3; lower panels: classical results. Contour lines $-0.05, -0.02, -0.01, 0.0, 0.03, 0.1, 0.2, 0.3, 0.4, 0.5, 0.6$ Ry. Solid (broken) lines non-negative (negative) values.

$$\phi = -4\pi\sigma_0 z (1 - R^3/r^3), \quad (1.21)$$

where σ_0 is the excess charge density far from the protrusion, z is the distance from the surface, and r is measured from the center of the protrusion. Locally, the excess charge redistributes itself into

$$\sigma = \sigma_0 (1 - R^3/r^3) \quad (1.22)$$

on the plane, and

$$\sigma = 3\sigma_0 z/R \quad (1.23)$$

on the sphere. We note that, at the boss apex, the electric field is three times its value at infinity.

To compare our quantum mechanical results with the classical theory, contained in (1.21)-(1.23), we approximate the adsorbed atom by a hemispherical boss with the radius chosen such that the zero equipotential lines coincide at the apex. One might be tempted to model an atom on a flat surface as a sphere rather than a hemispherical boss. Inspection of Fig.1.4, however, suggests that the latter is more appropriate. The result of the hemispherical model is also shown in Fig.1.4. Except on the sides of the adatoms, the agreement between the quantum mechanical result and classical one is quite good, at least at the semi-quantitative level. If we look at details, of course, there are some differ-

ences, which we show in Fig.1.5, where we plot the total external field strength along a line through the apex of the adatom. Comparing the fields in the presence and absence of the adatom, we again observe the expulsion of the field from the adatom region, which results in an enhancement of the field just outside the adatom. We note, however, that this field enhancement at the apex is not as much as classical theory predicts, i.e., a factor 3. Rather, the partial field penetration into the adatom results in a smearing out of the field as a reflection of the adjustability of the electronic distribution at the surface, reducing the enhancement effect. Note again, that for the heavier adatom, *Nb*, one is closer to the classical result. It is also noteworthy that, inside the bulk jellium, the Friedel oscillations are quite similar both with and without the adatom.

3.3 Core States

As we saw in Fig.1.5, there is a substantial expulsion of the electrostatic field from the region of the adatom. To understand the effect of an external electrostatic field on an adatom, we start from a bare metal in an external potential, $V_{ext}^M(r; F_0)$, due to the excess surface charge density σ_0 , producing an asymptotic field $F_0 = 4\pi\sigma_0$. When we bring an atom into this field, it will be polarized, producing an induced field with a potential $V_{ind}(r)$, which largely cancels the original field in the vicinity of the atom. Because the adatom is in close contact with the metal surface, there will, in addition, be a charge transfer from the atom

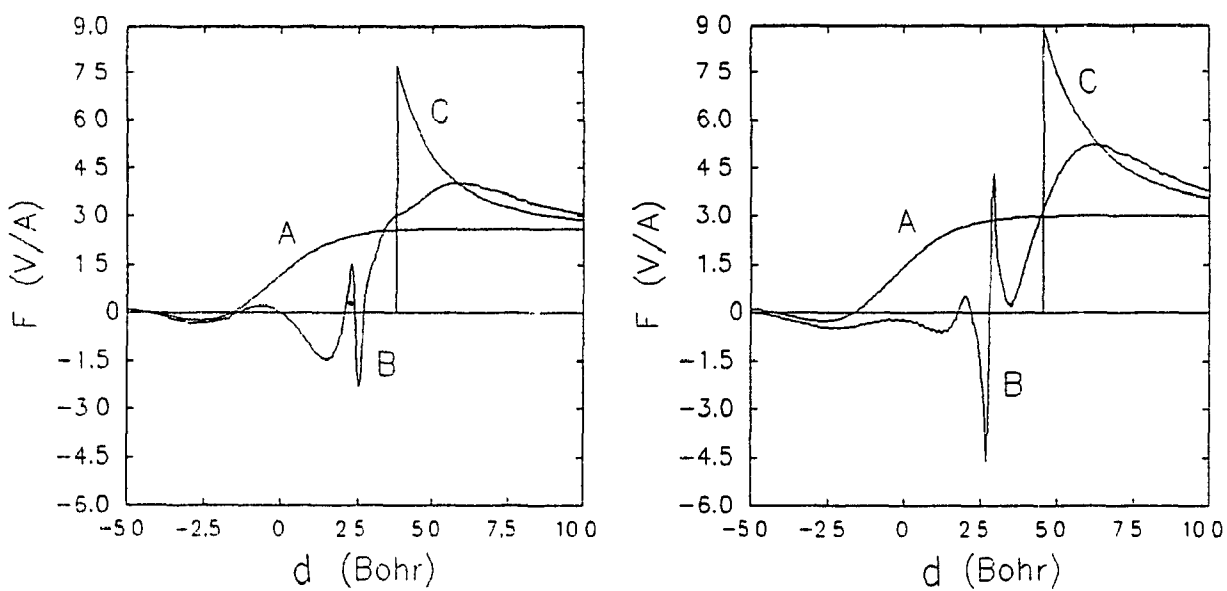


Fig.1.5: Electrostatic field strength along line through the center of the adatom for the same systems as in Fig.1.4. Curves *A* and *B*: without and with the adatom; curve *C*: classical result.

to the surface involving valence electrons of the adatom. This charge transfer also affects the core-level states, as demonstrated in Fig.1.6, where we plot the energy eigenvalue of the $1s$ level of an adsorbed Ti atom as a function of the adatom nuclear distance from the jellium edge, Z , for different field strengths. The energy eigenvalues, calculated within the framework of density-functional theory, do not directly give the energies required to remove an electron from the respective states. However, their distance dependence reflects the variation in the chemical shift. When the adatom is near the surface, there is a net transfer of electrons from the metal to the adatom, which generates more repulsion among electrons and causes the $1s$ level of the adatom to be higher than that of the isolated atom. As the adatom moves away from the surface, there is eventually some charge-draining to the surface, creating more attraction among electrons, so that the energy of the $1s$ level decreases. However, even at 4.0bohr, the $1s$ level of the adsorbed Ti atom is still above the $1s$ level of the Ti^+ ion.

The above effect suggests a way to assign a partial charge, q , to the adatom without the inherent arbitrariness connected with the Mulliken population analysis. To the lowest order, we set

$$\frac{q}{e} = \frac{E(1s) - E_0(1s)}{E_+(1s) - E_0(1s)} \quad (1.24)$$

where $E(1s)$, $E_0(1s)$ and $E_+(1s)$ are the energies of the $1s$ level of

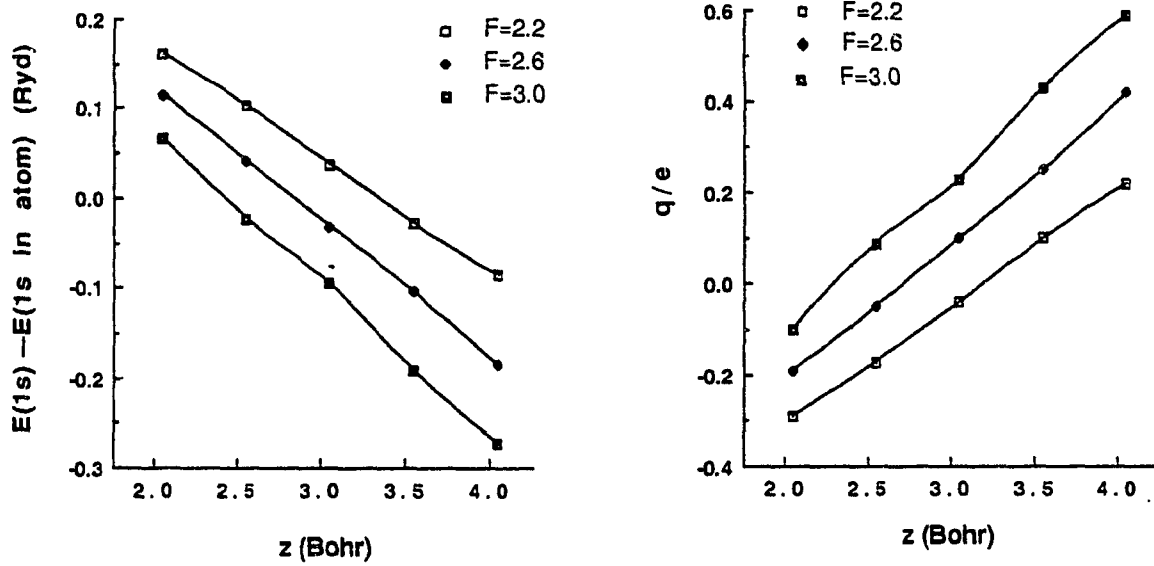


Fig.1.6: $1s$ energy levels and estimated charge, q , for Ti as a function of the adatom position from the jellium edge for different field strengths.

the adatom, isolated atom and isolated ion, respectively. This quantity is also plotted in Fig.1.6 as a function of the adatom position. We note that, at 4.0bohr these partial charges agree with the slopes, $-qF_0$, of the ground-state energy curves.

3.4 Dipole Moment

Experiments have been devised to extract the dipole moment and the polarisability of a metallic adatom from field emission work function changes³⁴. The dipole moment is rigorously defined in our theory as

$$\mu(F_0) = -e \int dr r [n^{MA}(r, F_0) - n^M(r, F_0) - Z\delta(r-R)], \quad (1.25)$$

where n^{MA} and n^M are the electron number densities with and without the adatom, respectively, and Z is the nuclear charge of the adatom at position R . We note that the total charge in the two situations are identical, both producing an asymptotic field F_0 . This guarantees that the definition (1.25) of the dipole moment does not depend on the origin chosen.

In the experimental literature, one parameterizes the dipole moment,

$$\mu(F_0) = \mu(F_0=0) + \alpha F_0, \quad (1.26)$$

in terms of the asymptotic field F_0 , defining the (field-dependent)

polarisability of the surface atom $\alpha(F_0)$, rather than introducing hyper-polarisabilities, gradient terms etc. Values of $\mu(F_0)$ and $\alpha(F_0)$ are given in Table 1.2. Measured polarisabilities³⁴ at field strengths $F_0 < 0.4V/\text{\AA}$ decrease monotonically from 11.94\AA^3 for *Ta* to 2.74\AA^3 for *Pt*. Our numbers for *Ti* and *Nb* are, indeed, close to that for *Ta*, an element with an atomic structure similar to *Ti* and *Nb*.

Tsong and Müller²⁵ have used the field-induced dipole moment of a metal atom at a kink site or on top of a close-packed plane to estimate the local field enhancement

$$F(r) = F_0 + \alpha(F_0) \frac{3n(F_0 \cdot n) - F_0}{r^3}. \quad (1.27)$$

Here F_0 is the constant electric field far from the surface and n is a unit vector in the direction of r . Along a line, perpendicular to the jellium surface and through the center of the adatom, the field from (1.27) is given by

$$F_z(z) = F_0 \left[1 + \frac{2\alpha(F_0)}{z^3} \right], \quad (1.28)$$

whereas the classical theory gives, from (1.21)-(1.23),

$$F_z(z) = F_0 \left[1 + \frac{2R^3}{z^3} \right]. \quad (1.29)$$

3.5 Conclusions

Table 1.2: Dipole moment, μ (in Debye), and polarizability, α (in \AA^3), at the equilibrium distance, as a function of field strength.

adatom		F_0 (V/\text{\AA})			
		2.2	2.6	3.0	3.4
<i>Ti</i>	μ	7.3	10.3	12.5	-
	α	9.9	11.9	12.4	-
<i>Nb</i>	μ	7.3	11.1	13.1	15.0
	α	10.1	12.8	13.1	13.3

We have presented self-consistent calculations of the electronic structure of *Ti* and *Nb* atoms adsorbed on a jellium metal in the presence of an external electric field. We have calculated ground-state energy curves, extracting activation energies for field evaporation and evaporation field strengths, and have found good agreement with the experimental data for the transition metals. Likewise, the calculated dipole moments and polarisabilities of these metallic adatoms are consistent with experimental values for other metals.

The field enhancement at kink sites, along steps, and above atoms in open surfaces, plays a crucial role in the image formation of the field ion microscope, as demonstrated by the fact that densely packed surfaces cannot be resolved. Our results show that a field enhancement by a factor of 1.5 to 2 must be expected $1-2\text{\AA}^0$ above an isolated metal atom. The implications of this effect for field adsorption of rare gases will be explored in the following section.

4. Field Adsorption of Rare Gas

4.1 Free Field Case

Initially, the weak physisorption of rare gas atoms on metal surfaces in the free electric field case was attributed to van der Waals forces, see, e.g., Ref.35. Using the jellium model of metals, which means that ionic cores smear into a uniform positive

background, and employing the method of Lang and Williams²⁸ for solving the Kohn-Sham single-electron equations of the density-functional formalism, Lang^{36,37} then demonstrated that one can also get good agreement with experimental binding energies, dipole moments and core-level shifts. The method of Lang and Williams contains an effective exchange-correlation potential which, in the local-density approximation²⁹, depends at each point only on the electron density at that point. Apart from the fact that the local-density theory includes electrostatic and kinetic-energy terms (and hence repulsive forces), it and the van der Waals picture differ simply in the degree of attachment envisaged between an electron and its exchange-correlation hole. Lang argued that since, for equilibrium rare gas atom-metal distances, the crucial part of the valence-shell electron orbit (that nearest the metal) lies sufficiently within the surface electron gas, the electron is most correctly considered to be attached to the hole.

4.2 Sharp Resonances

In the presence of external electric fields, the equilibrium rare gas-metal distances shorten, so that the method of Lang and Williams should work better. However, when a valence-electron orbit of the rare-gas atom is raised into the energy region of the valence band of the metal, it becomes a narrow resonance in the metal band. Narrow resonances within the conduction band were encountered by Lang for the heaviest rare gas, xenon³⁷. They cause self-consistent calculations to be rather tedious, as both reloca-

tion of the resonance peak and numerical integration over the resonance region become difficult.

The difficulties increase manifoldly for light rare gases in a field, e.g., the width of the resonance for *He* or *Ne* is about 10^{-4} eV for $F_0 = 3 \text{ V/\AA}$ and increases to 10^{-2} eV for $F_0 = 5 \text{ V/\AA}$. One remedy is to replace such sharp resonances by δ -functions in the early stages of the iteration, the finite width being incorporated only in the final approach to self-consistency.

Using a Green's function approach and the Anderson Hamiltonian³⁸, Newns³⁹ has derived the following expression for the density of states function,

$$f_L(\epsilon - \epsilon_a, \Gamma) = \frac{1}{\pi} \frac{\Gamma(\epsilon)}{(\epsilon - \epsilon_a)^2 + \Gamma^2(\epsilon)}. \quad (1.30)$$

If the energy dependence of Γ is ignored this is just a simple Lorentzian function of half width Γ centered around the position ϵ_a . To replace the sharp resonance of the electron state density, $\delta n(E)$, of, e.g., the $1s$ orbital of a *He* adatom by a δ -function, the resonance peak of $\delta n(E)$ is first approximated with a Lorentzian function, centered at E_{1s}^{MA} with a half width Γ , and, then, substituted with a δ -function,

$$\delta n'(E) = \delta n(E) - 2f_L(E - E_{1s}^{MA}, \Gamma) + 2\delta(E - E_{1s}^{MA}). \quad (1.31)$$

E_{1s}^{MA} and Γ are considered as parameters and optimized to smooth the function $\delta n(E) - 2f_L(E - E_{1s}^{MA}, \Gamma)$. The factors of 2 appearing in Eq.(1.31) account for spin degeneracy. The electron density distribution, $\delta n(r, E)$, is then approximated by

$$\delta n'(r, E) = \frac{\delta n'(E)}{\delta n(E)} \delta n(r, E). \quad (1.32)$$

4.3 Binding Distance and Desorption Energy

We now compare our calculations with the experimental results of field-induced adsorption of helium and neon on tungsten. The strengths of the external electric field, used in the calculation, are 0.0, 2.75, 3.30, 3.85, 4.40 and $4.95V/\text{\AA}$, or, when scaled by the evaporation field strength of tungsten, $F_{ev} = 5.6V/\text{\AA}$, they become $F/F_{ev} = 0.0, 0.5, 0.6, 0.7, 0.8$ and 0.9 , respectively. We have chosen $r_s = 3.0$ bohr for the jellium metal, appropriate to tungsten.

In Fig.1.7, we present the adsorption equilibrium distances calculated as functions of external electric field strengths and compare with the experimental data. Both the calculated and experimental adsorption equilibrium distances are measured from the image plane, z_{im} , which is half the separation distance between successive atom layers above the position of the first atom layer. The calculated desorption energies are compared with the corresponding experimental data in Fig.1.7 as well.

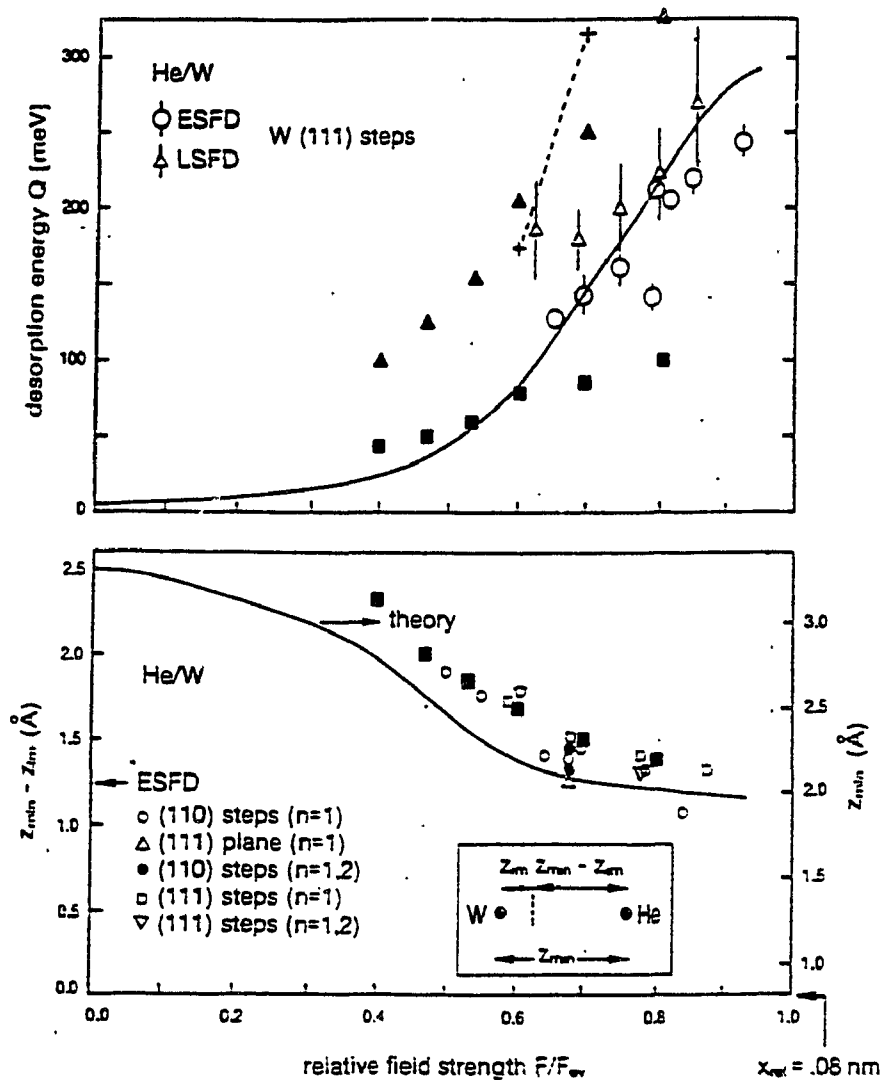


Fig.1.7: Desorption energies (upper panel) and binding distances (lower panel) of He field-adsorbed on W as a function of relative field strength F_0/F_{ev} with $F_{ev}=5.6V/\text{\AA}$. Experimental data labeled ESFD and LSFD from Ref.18,24, the calculated lines from Ref.20. Black squares are data with $\beta=1.5$, for desorption energies which are the lower limit estimates, while the upper limit estimates are indicated as black triangles. Crosses are data using M-T formula (1.36).

Comparison of calculated desorption energies and distances with experimental data is not straightforward and so needs some clarifying comments. We point out that Ernst's measurements yield values of the binding distance measured from the image plane. They must be corrected by the distance from the image plane to the atomic nucleus. We note that, in the low gas pressure limit of laser-induced thermal desorption, the desorption energy measured is most likely Q , the activation energy from the bottom of the adsorption well of the neutral adsorbate to the apex of the Schottky hump, where the neutral adatom is ionized, but not the binding energy of the neutral adatom, E_d . However, we should mention that in the present model, based on a variational principle, it is numerically very difficult to calculate the ground-state energy curve for the case, where the adsorbed atom is several angstroms away from the adsorption equilibrium distance. We therefore use the calculated energies to estimate the lower and upper limits of the desorption energies, for comparison with experimental desorption energies.

We first calculate the binding energy of a field adsorbed atom according to

$$E_b(Z, F) = E_{ad}(Z, F) - E^A(F), \quad (1.33)$$

where $E_{ad}(Z, F)$ is the energy of the adatom as defined in Eq.(1.12) and $E^A(F)$ is the energy of an isolated atom, i.e., far from the metal; all three are in a field of strength F . If the field

strength F is taken to be the asymptotic strength, F_0 , then the calculated binding distances are too large and the calculated binding energies are too low in comparison with the experimental data. One reason for this discrepancy is, no doubt, the lack of lattice structure in the jellium model. Our calculations are thus appropriate for field adsorption on a close-packed plane, whereas experiments clearly show that field adsorption of rare gases occurs preferentially above kink and edge atoms, where the field is significantly enhanced. The local field enhancement due to a single metal atom on an otherwise flat metal surface has been calculated using functional density theory in the local-density approximation, given in the preceding section. As revealed by Fig.1.5, a field enhancement of 20-50% occurs between 1.5 to 3.5 \AA above the metal atom. Alternatively, the enhancement can be estimated by approximating the metal atom on a close-packed plane with a spherical boss, of radius R , on a flat metal surface. For this geometry, the local field along a line through the apex of the boss and perpendicular to the surface is given by (1.29). We note, parenthetically, that the details of the electron distribution around the metal atom on a jellium surface suggest that a boss is a much better classical approximation than a sphere. As indicated in Fig.1.5, this model overestimates the field enhancement. This is also true for the Tsong-Müller²⁵ model, according to which the field above the polarized metal atom is given by (1.28). To account for the field enhancement, and thus make a meaningful direct comparison with experimental data, one should calculate the field adsorption of rare gases on top of a lone metal atom

adsorbed on a jellium surface. Unfortunately, such a calculation is not available at this time. We estimate the effect as follows: we assume that, around the minimum of the potential energy curve, the field is enhanced, from an asymptotic value F_0 to $F=\beta F_0$. The results of taking $F=\beta F_0$ with $\beta=1.5$ in (1.33) are shown as the black squares in Fig.1.7.

Whereas the calculated equilibrium binding distances agree well with experimental data, the calculated binding energies are still much lower than both the experimental desorption energies and earlier theoretical results¹⁸ obtained using the ASED-MO method. While the binding distance is a property at the minimum of the potential energy curve, the desorption energy is the energy difference between an adatom at the minimum, where the field strength is $F=\beta F_0$, and the adatom at the apex of the Schottky hump, where the field strength has some value between F_0 and βF_0 . Thus, we consider Eq.(1.33) as the lower-limit estimate of the desorption energy, while the following formula,

$$E_b(Z, F_0) = E_{ad}(Z, \beta F_0) - E^A(F_0), \quad (1.34)$$

defines its upper-limit estimate, the results of which are given as black triangles in Fig.1.7.

Similar comparisons for *Ne* are shown in Fig.1.8.

4.4 Electron Density Distribution

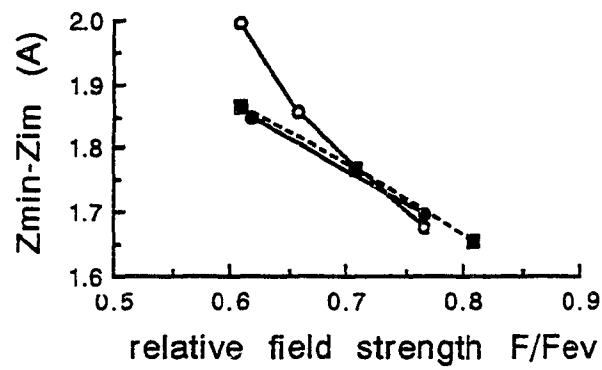
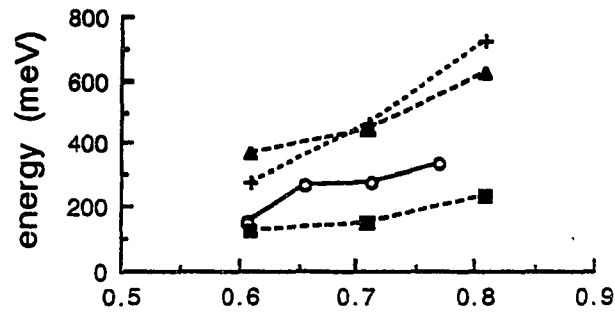


Fig.1.8: A figure for Ne similar to Fig.1.7. White circles and black ones are the experimental data from Ref.24, white ones being W(111)-step for $n=1$ and black ones W(111)-step for $n=1,2$. Other marks have the same meanings as those in Fig.1.7.

To understand the change in the bonding character as the electric field is increased, we look at the change in the electron density distribution,

$$\delta n(\mathbf{r}, F_0) = n^{MA}(\mathbf{r}, F_0) - n^M(\mathbf{r}, F_0) - n^A(\mathbf{r}, F_0), \quad (1.35)$$

where n^{MA} , n^M and n^A are the electron densities, in the presence of an electric field of asymptotic strength F_0 , of the coupled adatom-metal system at the equilibrium distance, the bare metal and the isolated atom, respectively.

In Fig.1.9, we plot δn for helium adsorbed on a jellium metal. In the left upper panel, we start with the field-free case, for which the changes are mainly due to the polarization of the $1s$ charge distribution, as discussed by Lang. With an increased field of $F_0/F_{ev}=0.6$, as in the right upper panel, further polarization, due to the excess positive charge on the metal surface, results in an induced dipole-dipole type interaction. The figure also indicates that, while some electron charge transfers from the outmost part of the adsorbed *He* atom, leading to a more attractive potential in the vicinity of the nucleus, there is a little increase of the electron density there. A further increase in the electric field, to $F_0/F_{ev}=0.7$ in the left lower panel and $F_0/F_{ev}=0.9$ in the right lower one, results in a charge transfer from the helium to the region between the adatom and the metal. This establishes a typical covalent bond and completes the transition from physisorption to field-induced chemisorption.

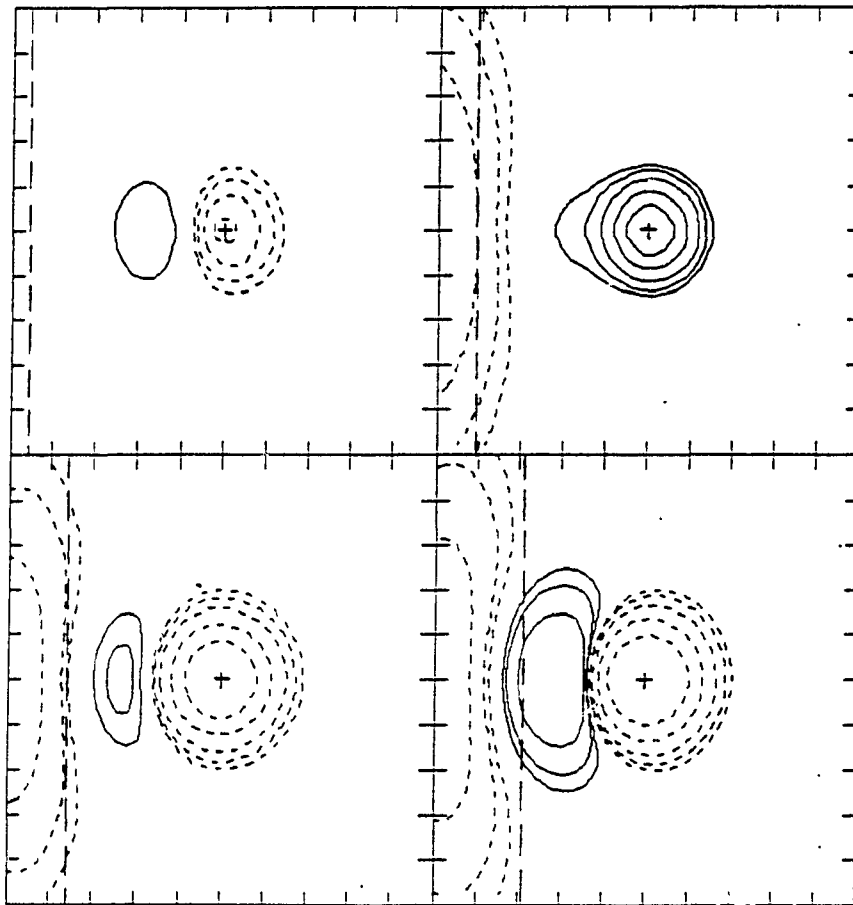


Fig.1.9: Electronic density shift for helium at the minimum, d , of the potential energy. For left-up, right-up, left-down and right-down, $d=5.0, 4.5, 4.0$ and 3.2 bohr and field strength $F/F_{ev}=0, 0.6, 0.7$ and 0.9 , respectively. Contours $\delta n = 0, \pm 0.00003, \pm 0.00005, \pm 0.0001, \pm 0.0003, \pm 0.001$ a.u. Solid (broken) lines non-negative (negative) values.

Similar figures for neon adsorbed on a semi-infinite jellium metal surface, with Wigner-Seitz radius $r_s=3.0$ bohr, are given in Fig.1.10. The left-up panel shows a polarized neon atom resulting from field-free adsorption. The right-up panel, for the case $F_0/F_{ev}=0.6$, shows that, while the $2p_x$ and $2p_y$ orbitals of the neon atom are contracted to the region near the nucleus, the outmost part of the electron density of the $2p_z$ orbital transfers from the neon to the surface. It represents the interaction of a more strongly polarized neon atom with the charged metal surface. In the left-down panel, for the case $F_0/F_{ev}=0.7$, there is some electron density accumulated in the region between the neon atom and the metal surface. The right-down panel, for the case $F_0/F_{ev}=0.8$, presents a typical weak chemisorption and completes the transition from physisorption to chemisorption.

In summary, high electric fields induce two simultaneous processes involving the valence orbitals of an adsorbed rare-gas atom: partial transfer of electron density from the rare-gas atom to the positively charged surface and redistribution of the electron density; the latter determines the adsorption-bond property.

4.5 Comments on Classical Models

Müller and Tsong^{23,25} proposed a phenomenological model of field adsorption of rare gases on metal tips in which the metal is represented by the single edge or kink atom on which field adsorption occurs. The external electric field is assumed to be

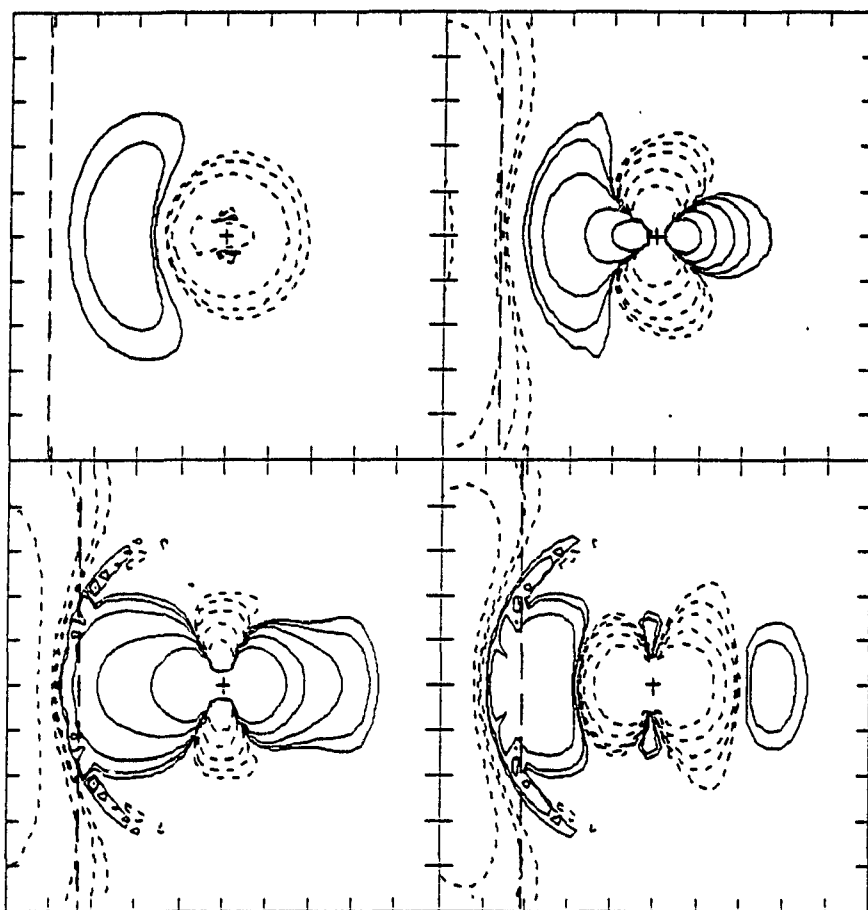


Fig.1.10: Electronic density shift for neon at the minimum, d , of the potential energy. For left-up, right-up, left-down and right-down, $d=4.5, 4.1, 3.7$ and 3.4 bohr and field strength $F/F_{cv}=0, 0.6, 0.7$ and 0.8 , respectively. Contours $\delta n = 0, \pm 0.00003, \pm 0.00005, \pm 0.0001, \pm 0.0003, \pm 0.001$ a.u. Solid (broken) lines non-negative (negative) values.

constant across the metal atom-rare gas atom dimer. The attraction then results from the interaction of the induced dipole moments of the two atoms, yielding a binding energy of

$$E_b = -\frac{1}{2}\alpha_a (f_a - 1)F_0^2, \quad (1.36)$$

where

$$f_a = \frac{(1+2\alpha_m/d^3)^2}{(1-4\alpha_m\alpha_a/d^6)^2}, \quad (1.37)$$

and where d is the distance between the metal atom and rare-gas atoms, α_a is the polarizability of the rare gas atom and α_m that of the metal atom. To fit data, Müller and Tsong^{23,25} take the low-field values for α_a and adjust α_m . There are also independent measurements of the polarizability of adsorbed metal atoms, which yield values of the right magnitude³⁴. The density functional calculations of the field adsorption of metal atoms on a jellium surface in the preceding section produce similar numbers and show, in addition, a strong dependence of α_m on the field strength. We should also point out that to get reasonable values for E_b from (1.36) one assumes that d is the sum of the van der Waals radii of the metal atom and rare gas, e.g., $d=(1.36+1.22)^0\text{Å}$ for helium on tungsten. Although the Tsong-Müller model is very appealing in its simplicity, the assumption that only a dimer consisting of a metal atom and a rare gas atom in a constant external field is considered to be oversimplified. There is also a question whether at such short distances a far field dipole picture is adequate to

estimate the binding energy.

Kreuzer *et al.* have recently worked out a first principles theory of dispersion and polarization interactions between an atom and a flat metal surface in high electric fields²⁶. For the dispersion or van der Waals energy one gets

$$V_{vdW}(z, F_0) = -\frac{C_3}{[z - z_d(F_0)]^3}, \quad (1.38)$$

where

$$C_3 = \frac{\hbar}{4\pi} \int_0^{\infty} \frac{\epsilon(i\omega) - 1}{\epsilon(i\omega) + 1} \alpha(i\omega) d\omega, \quad (1.39)$$

with α being the dynamic polarizability of the adatom and ϵ the dielectric function of the solid, both evaluated, using Kramers-Kronig relations, at imaginary frequencies; and $z_d(F_0)$ is the field-dependent position of the dynamic image plane. In addition, the polarization energy obtained is

$$E_{pol} = -\frac{1}{2} \alpha_0 F_0^2 - \frac{1}{32} \frac{\alpha_0^2 F_0^2}{[z - d_n(0, F_0)]^3}, \quad (1.40)$$

where α_0 is the static polarizability of the adatom and d_n is the position of the static image plane. Realistic estimates show that the binding energy of helium on a flat metal surface due to an induced dipole-dipole interaction is less than about 20meV. Natur-

ally, this theory does not account for the field enhancement above step and kink atoms, which, however, is not likely to amount to more than an order of magnitude.

A few years ago, Kreuzer *et al.* suggested that the dramatically increased binding energies of rare gases in external fields results from a transition from field-free physisorption to field-induced chemisorption^{1,16-18}. To understand field-induced chemisorption qualitatively, we assume for simplicity that the electric field is constant outside the image plane of the metal. Its presence then adds a term eF_0z to the potential energy of the system. To lowest order, this raises the adatom energy levels by an amount eF_0z_0 , where z_0 is the position of the nucleus of the adatom (in addition to adding off-diagonal elements, i.e., multipole moments). Considering helium as an example, we note that, in the absence of a field, the *He* $1s$ level (at -24.3eV) is well below the conduction band of the metal. As the electric field is increased, the $1s$ level will eventually move into the conduction band and become a (narrow) resonance state. At this stage, the adatom will also move closer to the metal, enhancing the wavefunction overlap and hence the binding, resulting in a continuous transition from physisorption to field-induced chemisorption with increased field strength.

Having the self-consistent electron distributions for field-adsorbed helium and neon, we can now calculate the electric moment of the adatom and the effective polarizability, according

to (1.25) and (1.26) respectively. We find, for relative field strengths up to $F_0/F_{ev}=1.0$, that the polarizability of adsorbed helium changes from 0.185\AA^3 to 0.211\AA^3 , i.e., comparable to the experimental low-field value of 0.205\AA^3 . A similar calculation for niobium on a jellium surface yields a polarizability of around 12\AA^3 . Although these values are of the correct order of magnitude, this does not justify classical models. Note that strong fields radically alter the electronic orbitals of field-adsorbed metal atoms and rare gases, leading to the establishment of adatom bonding orbitals with the surface. The corresponding dipole moments, written as effective charges separated by a distance, i.e., $\mu_z=q\ell$, are larger than that of the undisturbed atom. Thus, a far-field approximation to the dipolar field is not justified at the equilibrium position of adsorption. Nevertheless, if we use experimental values of the polarizabilities and adsorption distances in the Tsong-Müller formula (1.36), we get values of the binding energies that are far too large, see Figs.1.7 and 1.8. For example, for a *He* atom adsorbed on the apex of *W* surface atoms in a field of 4.5V/\AA , or $F_0/F_{ev}=0.8$, with the polarizabilities $\alpha_a=0.205\text{\AA}^3$ and $\alpha_m=4.6\text{\AA}^3$ for *He* and *W*, respectively, and an adsorption distance of $d=2.59\text{\AA}$, Tsong³¹ obtained a binding energy of 0.202eV, which agrees well with the experimental result. By contrast, using the measured polarizability of the adsorbed *W* atom, $\alpha_m=6.75\text{\AA}^3$ (Ref.34), and the adsorption distance $d=2.31\text{\AA}$ for *He* adsorbed on *W*(111) surface (Ref.24), we calculate the binding energy, according to Eq.(1.36), to be 0.538eV.

PART II: THERMAL FIELD-DESORPTION

1. Introduction

Thermal field-desorption is the removal of field-adsorbed species from the surface of a field ion tip which can be achieved by raising the temperature of the metal tip^{31,40,41}. Field evaporation, to be discussed in PART III, refers to the process of removing lattice atoms, as singly or multiply charged positive ions, from the surface of a field emitter tip in an electric field of the order of volts per angstroms^{42,43}. Both field evaporation and field desorption, crucial in the cleaning and preparation of field emitter tips, are thermally activated processes; as such, their rate constants can be parametrized according to Frenkel-Arrhenius as

$$r_d = \alpha \nu \exp(-Q(F)/k_B T). \quad (2.1)$$

Here, $Q(F)$ is the field dependent height of the activation barrier to be overcome by the desorbing particle, while ν can be identified with the vibrational frequency around the minimum, although it generally involves additional, temperature-dependent factors⁴⁴.

In thermal field-desorption both neutral and ionic species are removed. For the neutrals, which predominate at low field strengths (and, except alkali atoms and ions, are the only

desorbing species in free field), the additional factor in (2.1) is identified as the sticking coefficient, $\alpha=S$, which is a measure of the efficiency of energy transfer between the adsorbed particle and the solid. Although we have $S \approx 10^{-4}$ for helium in free field, some field dependence is to be expected in S . For desorbing ions, $\alpha=\alpha_i$ is a measure of the ionization probability for an adsorbed particle in its escape from the surface potential. This simplistic approach outlined above, however, ignores a number of interesting questions: whether the desorbing species emerge as ions or neutrals; whether post-ionization occurs; and what the energy distribution of the desorbing species is. To answer such questions Kreuzer *et al.*⁴⁵ proposed a kinetic theory which accounts for energy and charge transfers. They formulate the appropriate master equation for the problem and calculate all transition probabilities from first principles. Here, we will present detailed calculations of the kinetics of the thermal field-desorption of helium.

Field ionization results from the tunneling of electron from a gas particle in strong electric fields. If it occurs close to a metal tip, the emerging electron will tunnel directly into empty states above the Fermi level. This will happen predominantly in regions of locally enhanced electric fields, e.g., above kink sites, steps and single metal atoms on terraces, and can lead to image formation with atomic resolution. Of importance in formulating a theory is the fact that the approaching neutral particle is not in its ground state, which would be ionic and localized far from the tip, but rather is on an excited energy curve, which, far

from the tip, describes a neutral species isolated from the metal.

We start our discussion of field desorption by considering a helium atom adsorbed on a field ion tip. As the temperature is raised, the *He* atom will eventually get the chance to escape from its binding potential. If its escape from the surface is slow enough, it will get ionized at the hump of the ground-state energy curve and reach the detector as an ion. However, if ionization, i.e., the tunneling of an electron from the adatom to the metal, is too slow, the adatom will escape as a neutral atom with a kinetic energy unrelated to the ground-state energy curve. Indeed, a neutral atom in a field past a critical distance no longer corresponds to the ground state of the system, but rather to some excited state; the potential energy surface, describing such a neutral atom, is called diabatic.

From the above preliminary discussion, it should be obvious that the adiabatic states are not the most intuitive basis to set up a kinetic theory of field desorption and field ionization. Rather, a new basis must be constructed in which the charge state of the adsorbing species is identified and in which its motion is explicitly taken into account; they are called as diabatic states. Their construction from adiabatic states, including the identification of the coupling terms between them, will be reviewed in the next section. The diabatic states then form the starting point for the calculation of transition probabilities for ionization, which in turn will enter a master equation from which observables

like energy-dependent ion yields, the probability for post-ionization etc. can be computed. We should point out that, as any physical theory is inherently independent of the basis used, one could, of course, also formulate a kinetic theory of field desorption and field ionization starting from adiabatic states. However, a diabatic basis, in which neutral particles and ionic species are explicitly identified, has more intuitive appeal. Again, in this basis it is quite straightforward to identify electronically excited neutrals and ions and, if the gas particles are molecules, their vibrationally excited states. Correspondingly, in most phenomenological discussions of field desorption and field ionization, diabatic states have been the starting point.

2. Adiabatic and Diabatic States

2.1 Hamiltonian

We consider in front of a metal an atom at a distance R away from the topmost ion core. We will refer to this single atom as the adatom. For obtaining the adatom states, we fix, for the moment, the positions of the metal nuclei, i.e., we neglect the interaction between the adatom and the phonons of the metal. The Hamiltonian of this system can be written as

$$H_d = T_N + H_e(r_1, r_2, \dots; R), \quad (2.2)$$

where

$$T_N = -\frac{\hbar^2}{2M} \frac{\partial^2}{\partial R^2} \quad (2.3)$$

is the kinetic energy of the adatom nucleus, and

$$H_e = -\frac{\hbar^2}{2m} \sum_n \frac{\partial^2}{\partial r_n^2} + V_e(r_1, r_2, \dots; R) \quad (2.4)$$

is the Hamiltonian of the electrons at positions r_1, r_2, \dots . V_e includes the Coulomb interactions between the electrons, between the electrons and the nuclei, and between all nuclei (metallic and adatom's).

2.2 Adiabatic States

Let us fix the position of the adatom nucleus and set its kinetic energy (2.3) equal to zero. Physically, this assumes that the electronic degrees of freedom follow the nuclear motion instantaneously. We can then diagonalize H_e (in practice, after approximating it, e.g., by a tight-binding Hamiltonian, or using density-functional theory) to obtain

$$H_e(r;R) \zeta_i(r;R) = V_i(R) \zeta_i(r;R), \quad (2.5)$$

where the ζ_i are adiabatic many-electron wavefunctions. Here and below, we use r to represent all the electronic coordinates r_1, r_2, \dots . The lowest eigenvalue of (2.5), $V_0(R)$, represents the

ground state of the system and corresponds to the adiabatic binding energy curve. Lifting an electron, from the highest occupied level (in the ground state) to the lowest unoccupied one, generates the energy curve (or rather surface, because R is a three-dimensional space coordinate) of the first excited state etc.

To account for the nuclear motion of the adatom, we proceed now to construct diabatic states. We try to diagonalize the Hamiltonian (2.2) by solving Schrodinger's equation

$$H_d \Psi_\alpha = E_\alpha \Psi_\alpha \quad (2.6)$$

via the expansion

$$\Psi_\alpha(r;R) = \sum_i \zeta_i(r;R) \chi_{i\alpha}(R). \quad (2.7)$$

Inserting (2.7) into (2.6), multiplying by ζ_i^* and integrating over the electronic degrees of freedom, r , we obtain a set of coupled equations

$$\begin{aligned} & \left[-\frac{\hbar^2}{2M} \frac{\partial^2}{\partial R^2} + V_i(R) - E_\alpha \right] \chi_{i\alpha}(R) \\ & = \frac{\hbar^2}{2M} \sum_j \left(T_{ij}^{(2)} + 2 T_{ij}^{(1)} \frac{\partial}{\partial R} \right) \chi_{j\alpha}, \end{aligned} \quad (2.8)$$

where

$$T_{ij}^{(1)}(R) = \int \zeta_i^*(r;R) \frac{\partial}{\partial R} \zeta_j(r;R) dr \quad (2.9)$$

and

$$T_{ij}^{(2)}(R) = \int \zeta_i^*(r;R) \frac{\partial^2}{\partial R^2} \zeta_j(r;R) dr \quad (2.10)$$

are the matrix elements of the first and second order differential operators. Setting the right hand side of Eq.(2.8) equal to zero results in the Born-Oppenheimer approximation, according to which the nucleus moves only in the i th adiabatic potential.

Solving Eq.(2.8) amounts to obtaining an exact solution to the problem by diagonalizing an infinite matrix. To reduce the task to manageable proportions, one assumes that, in a given problem, only a limited number of adiabatic states contribute to the set of diabatic states involved in the process to be studied. For example, in field desorption and field evaporation, only the lowest diabatic states for a neutral atom and for ions appear important. They can thus be obtained from the corresponding adiabatic states by a unitary transformation. Since the latter are known explicitly from the tight-binding or density-functional calculations alluded to above, the problem is, in practice, solved.

2.3 Diabatic States

Let us introduce new states, η , with a transformation from the adiabatic states χ

$$\chi = A \eta, \quad (2.11)$$

where $\chi^T = (\chi_1, \chi_2, \dots)$ is the transpose of the column vector χ containing the adiabatic (nuclear) states as its components and A is a unitary matrix which is an explicit function of R . To obtain a diabatic solution of (2.8), we choose the transformation A such that the first-order derivative term vanishes, i.e., we impose the condition⁴⁶

$$\left(\frac{\partial}{\partial R} + T^{(1)} \right) A = 0. \quad (2.12)$$

We thus get from (2.8)

$$\left[-\frac{\hbar^2}{2M} I \frac{\partial^2}{\partial R^2} + W(R) - E \right] \eta = 0, \quad (2.13)$$

where η are diabatic states. In (2.13), I is a unit matrix, E is diagonal and the non-diagonal diabatic interaction matrix is given by

$$W = A^\dagger V A, \quad (2.14)$$

i.e., in terms of the adiabatic energy curves defined in (2.5). Dropping the coupling terms, W_{ij} , from (2.13) determines the uncoupled diabatic states, subject to

$$\left[-\frac{\hbar^2}{2M} \frac{\partial^2}{\partial R^2} + W_{ii}(R) - E_{i\nu} \right] \eta_{i\nu}^0 = 0. \quad (2.15)$$

Thus, $\eta_{i\nu}^0$ is the ν th eigenstate, with energy $E_{i\nu}$, of its diabatic potential $W_{ii}(R)$. For example, W_{00} would be the potential for a neutral atom approaching a surface and W_{11} that of an ion. The off-diagonal terms, W_{ij} , couple these states together; in the above example, W_{01} is responsible for ionization or neutralization.

Combining (2.7) and (2.11), we can rewrite the total wavefunction as

$$\begin{aligned} \Psi_\alpha(r;R) &= \sum_i \zeta_i(r;R) \chi_{i\alpha}(R) \\ &= \sum_i \zeta_i(r;R) A_{ij}(R) \eta_{j\alpha}(R) \\ &= \sum_j \xi_j(r;R) \eta_{j\alpha}(R), \end{aligned} \quad (2.16)$$

by introducing the diabatic many-electron wavefunctions, $\xi^T(r;R) = (\xi_0, \xi_1, \dots)$.

2.4 Two-State System

Before continuing with the explicit calculation of adiabatic and diabatic states, we briefly discuss their meaning. To this end, we assume that only two levels participate in the process of

field desorption, while the other electronic levels remain unchanged, acting as spectators throughout the process. We denote by ϕ_a the highest occupied single-electron level with energy ϵ_a in the isolated adatom and by ϕ_m the lowest unoccupied level of the same symmetry with energy ϵ_m above the Fermi energy of the isolated metal. In the interacting system of adatom plus metal, these two levels combine to form two molecular orbitals, Φ_g and Φ_e , of lower and higher energy, respectively; see Fig.2.1. Assuming that we can approximate the adiabatic many-electron wavefunctions as Slater determinants, we find that the adiabatic ground wavefunction for N electrons,

$$\zeta_0(r;R) = | \Phi_1 \Phi_2 \dots \Phi_{N-1} \Phi_g | , \quad (2.17)$$

is composed of the spectator states, Φ_i where $i=1, \dots, N-1$, and Φ_g , while the adiabatic, excited many-electron wavefunction,

$$\zeta_1(r;R) = | \Phi_1 \Phi_2 \dots \Phi_{N-1} \Phi_e | , \quad (2.18)$$

has Φ_g replaced by Φ_e . If one assumes, with the adatom close to the metal, that ϵ_a is lower than ϵ_m , then Φ_g and Φ_e are dominated by ϕ_a and ϕ_m , respectively. Thus, ζ_0 represents a many-electron wavefunction in which both adatom and metal are in their respective neutral ground states, whereas ζ_1 describes a situation with an

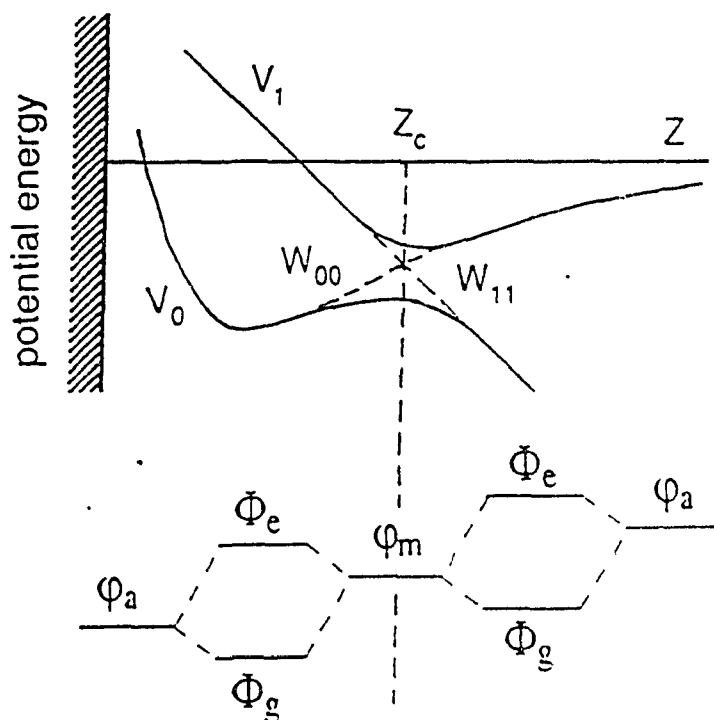


Fig.2.1: Adiabatic (V_i) and diabatic (W_{ii}) potential energy curves and schematic drawing of noninteracting (ϕ_a and ϕ_m) and interacting (Φ_g and Φ_e) orbitals to illustrate the discussion around Eqs.(2.17) and (2.18).

electron transferred from the adatom to the lowest empty orbital of the metal. When the adatom moves far from the metal, ϵ_a is raised by the external electric field such that it is higher than ϵ_m , and so Φ_g and Φ_e are dominated by ϕ_m and ϕ_a , respectively. In this case, the adiabatic ground wavefunction ζ_0 describes a situation in which an electron is transferred from the adatom to the metal, whereas the adiabatic, excited wavefunction ζ_1 represents a many-electron state in which both adatom and metal are in their respective neutral ground states.

In Ref.7, we have shown that, for two relevant states, the transformation A in (2.11) can be represented by a unitary 2x2 matrix, which can be written, quite generally, as

$$A = \begin{bmatrix} \cos\theta(R) & \sin\theta(R) \\ -\sin\theta(R) & \cos\theta(R) \end{bmatrix}. \quad (2.19)$$

Noting that the matrix $T^{(1)}$ is antisymmetric, we reduce the matrix equation (2.12) to a simple vector equation,

$$\begin{aligned} \frac{\partial}{\partial R} \theta(R) &= - \langle \zeta_0 \left| \frac{\partial}{\partial R} \right| \zeta_1 \rangle \\ &= - \int \zeta_0^*(r;R) \frac{\partial}{\partial R} \zeta_1(r;R) dr, \end{aligned} \quad (2.20)$$

which can be solved as a line integral,

$$\theta(R) = - \int_{R_0}^R \langle \zeta_0 | \frac{\partial}{\partial R} | \zeta_1 \rangle \cdot dR' . \quad (2.21)$$

Setting $\theta(R_0)=0$ implies that $A(R_0)=I$, and thus that, at R_0 , diabatic and adiabatic states coincide, as is the case far from the surface. The diabatic interaction matrix (2.14) is now given explicitly by its components:

$$W_{00}(R) = \cos^2\theta(R) V_0(R) + \sin^2\theta(R) V_1(R); \quad (2.22)$$

$$W_{11}(R) = \cos^2\theta(R) V_1(R) + \sin^2\theta(R) V_0(R); \quad (2.23)$$

and

$$W_{01}(R) = \frac{1}{2} \sin 2\theta(R) [V_0(R) - V_1(R)]. \quad (2.24)$$

To evaluate (2.21), we first observe that, in field desorption, adatoms will leave the surface along the steepest field gradient, i.e., perpendicular to the surface. Hence, we can neglect any lateral interactions and assume that $\theta=\theta(Z)$ depends only on the distance Z from the metal, which yields

$$\theta(Z) = - \int_{\infty}^Z dZ \int dr \Phi_g(r;Z) \frac{\partial}{\partial Z} \Phi_e(r;Z), \quad (2.25)$$

provided that the adiabatic many-electron wavefunctions are given by Slater determinants. This completes the construction of dia-

batic states for situations in which only two states are important. We should note, however, that, even in the case of thermal field-desorption of helium, this is not strictly correct. Recall that field ionization of the adatom can take place when its highest occupied level rises above the lowest unoccupied level in the metal. For a given field strength, F , this happens if the adatom is at a distance $Z_c(F)$. If the desorbing atom is at distances Z larger than Z_c , the electron can tunnel into higher unoccupied levels of the metal. Thus, for given F and Z , only two states participate in the ionization process and hence in the construction of diabatic states, although a band of metal states is relevant in the overall field desorption process. Note, however, that because the tunneling probability decreases rapidly as a function of distance, this band of tunneling states is rather narrow. Mimicking the metal by a finite cluster of metal atoms obviously does not produce a band structure, but rather a set of discrete levels, which one has to broaden with a width corresponding to the width of the ionization zone.

In Fig.2.2, we present adiabatic and diabatic potential energy curves for a *He* atom adsorbed on a *W* surface in a field of two different strengths. Such curves have been drawn qualitatively to serve as a basis for Müller's image-hump model^{42,43}, Gomer's charge-exchange model^{47,48}, and discussions of charge-hopping and charge-draining mechanisms^{2,49}. According to the discussion above, the difference between the adiabatic potential energy curves reaches a minimum at the apex and is of the order of the

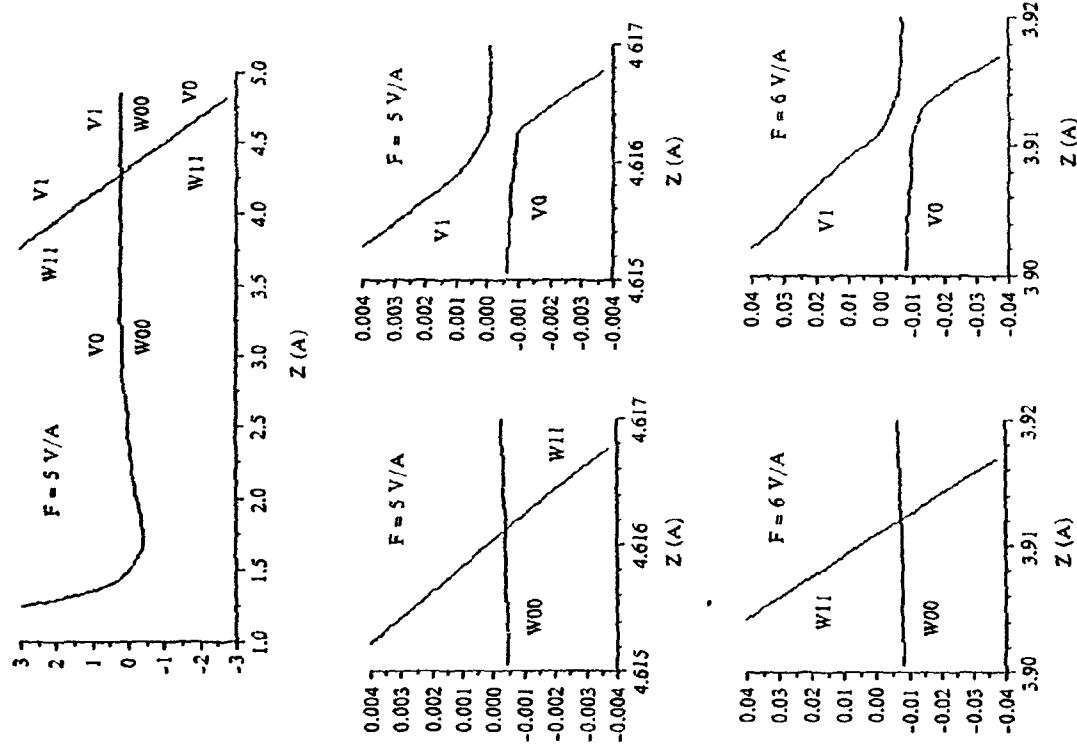


Fig.2.2: Adiabatic (V) and diabatic (W) energy curves for He on W in a field of $5V/\text{\AA}$ (upper set and enlarged version in center) and of $6V/\text{\AA}$ (lower set).

interaction energy between the highest occupied and the lowest unoccupied orbitals. With increasing field, the apex will move towards the metal surface, resulting in an increase in the interaction energy and thus in an increase in the energy difference between the adiabatic energy curves. We note that θ varies rapidly from 0° to 90° over a very short distance, i.e., less than 0.1 \AA around the apex of the adiabatic ground-state energy curve, which indicates the narrowness of the ionization zone.

3. Kinetics

3.1 Uncoupled States and Coupling Terms

To calculate the kinetics of field desorption and field ionization, the relevant kinetic equation must be formulated to properly account for the processes of energy- and charge-exchange. We supplement the Hamiltonian, describing diabatic states, H_d , with both a Hamiltonian, H_s , describing the thermal degrees of freedom of the metal, and a coupling term, H' , to write

$$H = H_d + H_s + H' . \quad (2.26)$$

A transparent way to describe systems in which the number of the particles changes as a function of time is via creation and annihilation operators. We first note that the field operator $\Psi(R, t)$, describing I diabatic states, can be represented as an I -dimen-

sional vector with components $\Psi_i(R, t)$. We expand the $\Psi_i(R, t)$ in terms of the uncoupled diabatic eigenstates defined in (2.15), i.e.,

$$\Psi_i(R, t) = \sum_{\nu} a_{i\nu}(t) \eta_{i\nu}^0(R). \quad (2.27)$$

In the above equation, we have introduced the annihilation operators $a_{i\nu}$, that destroy a neutral or ionized particle of the i th species in the ν th state of its diabatic potential W_{ij} , with their Hermitian conjugates being the creation operators $a_{i\nu}^+$. We thus have

$$\begin{aligned} H_d &= H_d^0 + H'_d \\ &= \sum_{i\nu} E_{i\nu} a_{i\nu}^+ a_{i\nu} + \sum_{ij\nu\mu} \langle j\mu | W_{ji} | i\nu \rangle a_{j\mu}^+ a_{i\nu}, \end{aligned} \quad (2.28)$$

where the off-diagonal terms W_{ij} were introduced in (2.14).

For the thermal degrees of freedom of the metal, we assume that harmonic phonons are a good approximation and write

$$H_s = \sum_J \bar{n} \omega_J b_J^+ b_J, \quad (2.29)$$

where b_J annihilates a phonon of mode J with energy $\bar{n}\omega_J$. In principle, the phonon modes should be constructed for the tip geometry, including local modes specific to the particular surfaces at which

field desorption is being studied. This is a rather complicated task, but, fortunately, it has been shown in the theory of thermal desorption³⁵ that such local surface modes do not introduce qualitatively new features into the desorption kinetics, since the thermal desorption rate constant is an integral over all participating phonon modes. Thus, one obtains the rate constant, within a factor of 2 or 3, by using bulk phonon modes, $J = (\sigma, k)$, where σ denotes the polarization vector of the transverse and longitudinal phonon modes and k the wavevector. In any case, the coupling term for energy exchange between the adatom and the phonons of the solid reads

$$H' = \sum_{i\nu\mu J} X_i(\nu, \mu; J) a_{i\nu}^+ (b_J^+ + b_J) a_{i\mu}, \quad (2.30)$$

where the matrix elements are given by

$$X_i(\nu, \mu; J) = - \sqrt{\frac{\hbar}{2\rho_0\omega_J}} \int dR \eta_{\nu}^{0*}(R) u_J \cdot \frac{\partial W_{ii}(R)}{\partial R} \eta_{\mu}^0(R), \quad (2.31)$$

and u_J is the normal phonon mode; further details can be found, e.g., in Ref.35.

3.2 Master Equation

Starting from $H_d^0 + H_s$ and using $H'_d + H'$ as a perturbation, Tsukada and Gortel⁵⁰ have recently derived a generalized master equa-

tion that controls the kinetics of field adsorption and field desorption and takes into account non-Markovian effects. With the introduction of the occupation probabilities for an adatom of kind i to be in state ν of its diabatic potential W_{ii} ,

$$n_{i\nu}(t) = \langle a_{i\nu}^\dagger a_{i\nu} \rangle, \quad (2.32)$$

the master equation in the Markovian limit reads

$$\begin{aligned} \frac{dn_{i\nu}}{dt} = & \sum_{\mu} [R_i(\nu, \mu) n_{i\mu} - R_i(\mu, \nu) n_{i\nu}] \\ & + \sum_{\mu^j} [T_{ij}(\nu, \mu) n_{j\mu} - T_{ji}(\mu, \nu) n_{i\nu}]. \end{aligned} \quad (2.33)$$

The phonon transition rates, in the one-phonon approximation, are given by Ref.35 as

$$\begin{aligned} R_i(\nu, \mu) = & \frac{2\pi}{\hbar} \sum_J |X_i(\nu, \mu; J)|^2 [n^{(ph)}(\omega_J) \delta(E_{i\nu} - E_{i\mu} - \hbar\omega_J) \\ & + (n^{(ph)}(\omega_J) + 1) \delta(E_{i\nu} - E_{i\mu} + \hbar\omega_J)] / \omega_J, \end{aligned} \quad (2.34)$$

where $n^{(ph)}$ are the Bose-Einstein phonon occupation functions.

For the tunneling rates, a straightforward generalization of the expression obtained by Tsukada and Gortel⁵⁰ to systems with more than two relevant states gives

$$T_{ij}(\nu, \mu) = \frac{2\pi}{\hbar} \left| \int dR \eta^{0*}_{i\nu}(R) W_{ij}(R) \eta^0_{j\mu}(R) \right|^2 \Delta(E_{i\nu}, -E_{j\mu}, \Gamma_{j\mu}), \quad (2.35)$$

with

$$\Delta(\epsilon, \Gamma) = \frac{1}{\pi} \frac{\Gamma/2}{\epsilon^2 + \Gamma^2/4}. \quad (2.36)$$

In (2.35), $\Gamma_{j\mu}$ is the half-width of level μ in the j th diabatic potential, W_{ij} , due to phonon transitions and is given via (2.34) as

$$\Gamma_{j\mu} = \hbar \sum_{\nu} R_j(\nu, \mu). \quad (2.37)$$

Because $T_{ij}(\nu, \mu)$ describes transitions between discrete states of the unperturbed Hamiltonian, care must be exercised to include the width of the initial state. This is done formally by replacing the energy-conserving δ -function by the Lorentzian (2.36).

4. Discussion

4.1 Ion Yield

The kinetics of a gas atom interacting with a metal under high-field conditions is described by the master equation (2.33) for the time evolution of the occupation functions $n_{i\nu}$ for a particle of kind i in the ν th state of its diabatic potential W_{ij} . Here i labels

ground-state neutral atoms, singly or multiply charged ions, as well as electronically excited neutrals or ions.

To be more specific in our discussion we denote in the master equation (2.33) neutrals and singly and doubly charged ions by the subscripts 0, + and ++, respectively. We get for the neutral species

$$\begin{aligned} \frac{dn_\nu^0}{dt} = & \sum_{\mu} [R_0(\nu, \mu) n_{\mu}^0 - R_0(\mu, \nu) n_{\nu}^0] \\ & + \sum_{\mu} [T_{0+}(\nu, \mu) n_{\mu}^+ - T_{+0}(\mu, \nu) n_{\nu}^0] \\ & + \sum_{\mu} [T_{0,++}(\nu, \mu) n_{\mu}^{++} - T_{++,0}(\mu, \nu) n_{\nu}^0]. \end{aligned} \quad (2.38)$$

Let us assume for the moment that ν refers to a bound state of a neutral atom bound in W_{00} to the surface of the metal. For μ also referring to bound states, we note that the first sum contains phonon-assisted transitions between these bound states in W_{00} ; usually much faster than other transitions, they maintain a quasi-equilibrium in the adsorbate as the system evolves in time. If in the first sum the μ refer to continuum states in W_{00} , the first (second) term gives the rate of thermal adsorption (desorption). If ν refers to a continuum state, one then has continuum-continuum transitions corresponding to surface scattering of neutral species without altering the electronic configuration.

The second sum in (2.38) contains reneutralization of singly charged ions (first term) and creation of singly charged species (second term). Again, these transitions can involve adsorbed particles (bound states of W_{ii}) or gas-phase particles (continuum states of W_{ii}). For example, terms involving T_{+0} (μ =continuum states, ν =bound state) describe the ionization of an adsorbed particle leading to field desorption, whereas T_{+0} (μ =continuum state, ν =continuum state) leads to the ionization of a neutral particle approaching the tip from the gas phase. The last sum in (2.38) then describes the equivalent processes involving doubly charged ions.

Let us now implement conditions of thermal desorption in (2.38), considering helium as an example. Experimentally, one field-adsorbs helium at low temperature and with fields of around $4V/\text{\AA}$, resulting in helium atoms bound in the lowest state of W_{00} . Fast heating of the tip, e.g., by a laser pulse, leads to rapid population of the higher states of W_{00} followed by thermal desorption and ionization. Re-adsorption and reneutralization are negligible if the temperature rise is fast enough; Eq.(2.38) then simplifies to

$$\frac{dn_{\nu}^0}{dt} = \sum_{\mu} [R_0(\nu, \mu) n_{\mu}^0 - R_0(\mu, \nu) n_{\nu}^0] - \left[\sum_{k_0} R_0(k_0, \nu) + \sum_{k_+} T_{+0}(k_+, \nu) + \sum_{k_{++}} T_{++0}(k_{++}, \nu) \right] n_{\nu}^0,$$

(2.39)

where we imply that ν and μ refer only to bound states in W_{00} , with continuum states of neutrals, and singly and doubly charged ions denoted by k_0 , k_+ and k_{++} , respectively. For neutral atoms in the continuum, we get

$$\frac{dn_{k_0}^0}{dt} = \sum_{\nu} R_0(k_0, \nu) n_{\nu}^0. \quad (2.40)$$

Similarly, for the ions, we obtain

$$\frac{dn_{k_+}^+}{dt} = \sum_{\nu} T_{+0}(k_+, \nu) n_{\nu}^0 - \sum_{k_{++}} T_{++,+}(k_{++}, k_+) n_{k_{++}}^+, \quad (2.41)$$

and

$$\frac{dn_{k_{++}}^{++}}{dt} = \sum_{\nu} T_{++,0}(k_{++}, \nu) n_{\nu}^0 + \sum_{k_+} T_{++,+}(k_{++}, k_+) n_{k_+}^+. \quad (2.42)$$

The last sums in (2.41) and (2.42) correspond to post-ionization of singly charged species.

To solve Eqs.(2.39)-(2.42), we recall that phonon-assisted transitions within the surface potential W_{00} of the neutral species are typically much faster than any other process considered.

The first sum in (2.39), therefore, very nearly cancels, keeping the remaining adsorbed atoms in quasi-equilibrium throughout the desorption process. We can therefore solve (2.39) with an ansatz⁵⁰,

$$n_i^0(t) = A \exp(-E_{0i}/k_B T) \exp(-\lambda t). \quad (2.43)$$

The rate constant is given by

$$\lambda = \frac{\sum_{\nu} \left[\sum_{k_0} R_0(k_0, \nu) + \sum_{k_+} T_{+0}(k_+, \nu) + \sum_{k_{++}} T_{++10}(k_{++}, \nu) \right] \exp(-E_{0\nu}/k_B T)}{\sum_{\nu} \exp(-E_{0\nu}/k_B T)} \quad (2.44)$$

where the first term corresponds to loss of atoms in the adsorbate due to thermal desorption, the second is due to formation of singly charged ions and the last is due to direct double-ionization. With (2.43), Eqs.(2.41) and (2.42) can be integrated without difficulty.

To establish the connection with experimentally observable quantities, note that the particle flux observed in a detector is proportional to the rate of formation, determined by Eqs.(2.40)-(2.42). Thus, we find for the yield of singly charged ions,

$$Y_{ion} = \frac{\sum_{\nu, k_+} T_{+0}(k_+, \nu) \exp(-E_{0\nu} / k_B T)}{\sum_{\nu} \exp(-E_{0\nu} / k_B T)}, \quad (2.45)$$

keeping in mind that the energy of the detected particle is given by $E = \hbar^2 k^2 / 2M$ in terms of the quantum label k (wavevector) of the continuum states.

To determine the transition probability in (2.45) from (2.35), we must know the nuclear unperturbed diabatic states, $\eta_{0\nu}^0$ and $\eta_{+k_+}^0$, in the diabatic potentials, W_{00} and W_{++} . To simplify the numerics, we have fitted a Morse potential to W_{00} :

$$W_{00}(Z) = A_0(F) \{ \exp[-2\gamma(Z-Z_0)] - 2 \exp[-\gamma(Z-Z_0)] \}, \quad (2.46)$$

adjusting its parameters, $A_0(F)$, $\gamma(F)$ and $Z_0(F)$, as functions of field strength. Likewise, we set

$$W_{++}(Z) = W_c - eF(Z-Z_0) \quad (2.47)$$

for the diabatic curve of the ion. For both potentials, the unperturbed diabatic states can be derived analytically.

4.2 Thermal Desorption of Helium

In Fig.2.3, we show the ion yield as a function of flight time, adjusted in position and height to allow direct comparison with the experimental data by Tsong⁵¹. We note that the theoretical curve has an energy width of about 0.6eV as compared to about 1eV in the experiment. In view of the number of theoretical approximations, these two estimates compare rather favorably.

Thermal field-desorption being an activated process, we have evaluated the yield (2.45) according to the Frenkel-Arrhenius parametrization of (2.1). The results, together with the position of adsorption, are presented in Fig.2.4 as functions of field strength. We take the electric field from self-consistent calculations using density-functional theory performed at flat surfaces^{10,11}. Representing tungsten, a transition metal, by an inherently approximate r_s value introduces some uncertainties into the theory. To estimate the reliability of this procedure, we present the results in Fig.2.4 for two values of r_s : 1.5 and 2.0. The theory is definitely not more accurate than the spread in data points; this is the best we can do with our present, rather crude, cluster programme based on the ASED-MO method.

The lowest panel in Fig.2.4 reveals an interesting qualitative feature, that is, the dramatic, roughly exponential, increase in the prefactor as a function of field. We recall that in ordinary, or field-free thermal desorption, the effective prefactor is the product of a sticking coefficient and a desorb-attempt frequency. In thermal field-desorption, the role of the sticking coefficient

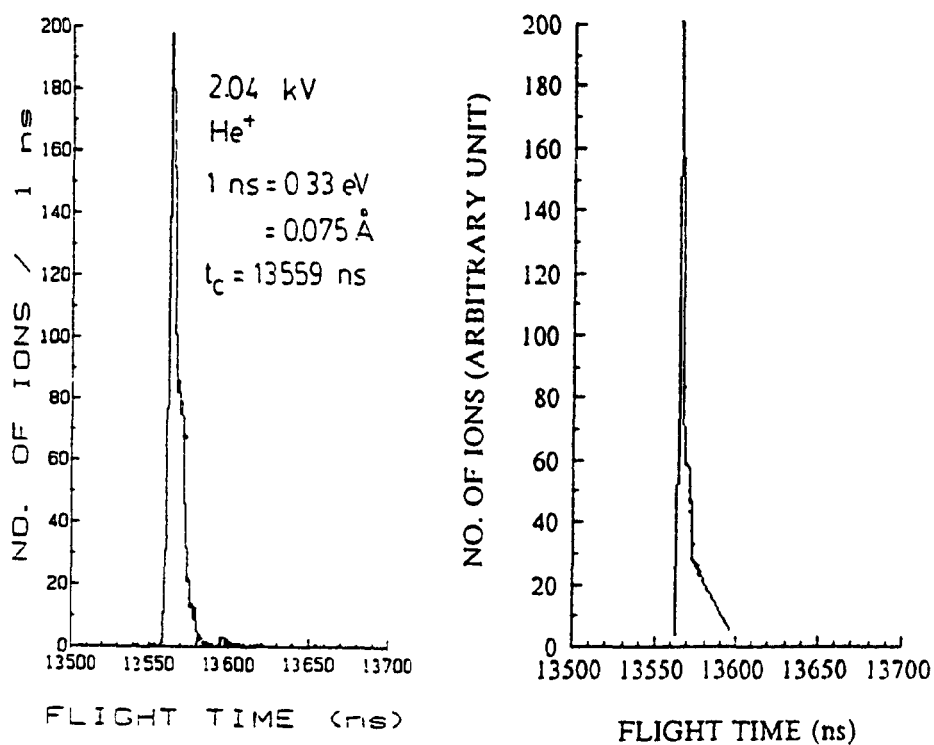


Fig.2.3: Time of flight for *He* field-desorbed from *W* at $4.5V/\text{Å}$ at $T=160\text{K}$. Left curve: experimental result from Ref.51; right curve: calculation from (2.45) with peak position and height adjusted for comparison with the experimental result.

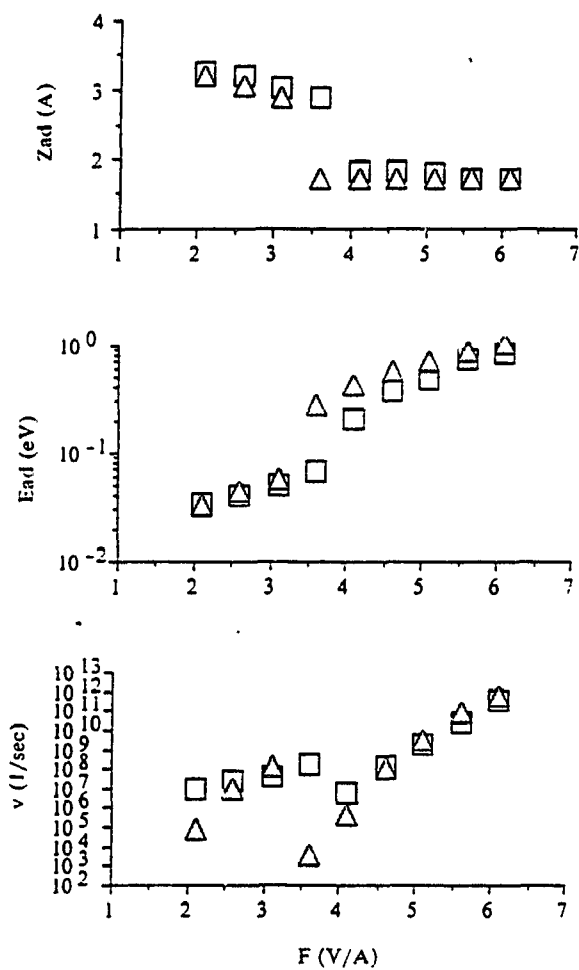


Fig.2.4: Position of field-adsorbed He , z_{ad} , activation energy, E_d , and prefactor, ω , as a function of field strength. Local fields from density functional calculations with $r_s=1.5$ (squares) and 2.0 (triangles).

is replaced by the ionization probability at the apex of the adiabatic ground-state energy curve. It varies from zero in $F=0$ to a saturation limit in high fields, as borne out by our calculations. For *He*, this strong field-dependence of the prefactor has an interesting consequence. We note that, for *He*, the activation energy for field desorption is roughly equal to the depth of the diabatic curve for the neutral species. Thus, thermal field-desorption of neutral and ionic *He* have the same desorption energy, implying that the ratio of ions to neutrals is proportional to the ratio of the prefactors. Because the prefactor for the desorption of neutral *He* is not strongly dependent on field strength, we predict that the ratio of ion to neutral yield is an exponential function of field strength. In particular, well below the best image voltage, thermal desorption will only yield neutral *He*. To test this idea, an experiment should start from a well-defined, constant coverage of *He*, which is then totally removed by a fast temperature rise so that the total number of desorbed species remains constant. If the detector registers only ions, one should see the exponential increase in ion yield directly.

5. Conclusions

Hopefully, we have demonstrated that the theory presented in this part contains the relevant ingredients for a complete description of the kinetics of field desorption, field evaporation and field ionization. It should also be obvious by now that a successful theory cannot start by modeling the various rates in the

master equation (2.33). Rather, they must be calculated from first principles, as alluded to in the introduction. Only on the basis of such calculations will it be possible to answer such questions as to: whether post-ionization is important in a given system or not; how wide the ionization region is; and what temperature and energy dependence the emerging ions will have.

In this part, we have calculated the yield of singly charged ions in a thermal field-desorption experiment. It appears to us that, using the master equation approach, one could eventually also tackle the much more complicated problem of image formation in the field ion microscope.

PART III: FIELD EVAPORATION OF METALS

1. Introduction

Induced by electric fields of order of volts per angstroms, field evaporation is a thermally activated process, involving the removal of lattice atoms, as singly or multiply charged positive ions, from the surface of a field emitter tip. In the Frenkel-Arrhenius or Polanyi-Wigner parametrization of its rate constant (Eq. (2.1))

$$r_d = \alpha \nu \exp(-Q(F)/k_B T), \quad (3.1)$$

where $Q(F)$ is again the field-dependent desorption activation-barrier height and the prefactor is split into an attempt frequency, ν , and an accommodation coefficient, α , both being field- and also weakly temperature-dependent. The evaporation field strength, or minimum field strength beyond which the activation barrier vanishes and field evaporation at low temperatures occurs, varies from $2.5V/\text{\AA}$ for *Ti* to $6.1V/\text{\AA}$ for *W*, with typical experimental errors margin of 10-20%³¹. Ernst⁵³ has measured $Q(F)$ and $\nu(F)$ for *Rh*, and Kellogg³² has presented data for *W* in the field range $4.7-5.9V/\text{\AA}$.

Two phenomenological models have been proposed to calculate the activation energy $Q(F)$: the "image-force" model and "charge-

exchange" model. In the "image-force" model^{42,43} field evaporation is envisaged as the activation of an ion of charge ne over an activation barrier that results from the superposition of the field potential, $-neFZ$, (assuming a constant electric field), and the image potential of the ion, $-ne/4Z$. One gets

$$Q(F) = \Lambda + \sum_n I_n - n\Phi - \sqrt{n^3 e^3 F} + \frac{1}{2} (\alpha_a - \alpha_i) F^2, \quad (3.2)$$

where Λ is the field-free sublimation (cohesive) energy of the metal, I_n is the n th ionization potential of the desorbing ion, Φ is the work function of the surface, F is the applied electric field strength, and α_a and α_i are the polarizabilities of the surface and the desorbing atoms, respectively. In the "charge-exchange" model⁴⁷, one assumes that ionization and desorption occur at the crossover point Z_c between the atomic and ionic (adiabatic) potential energy curves. One finds

$$Q(F) = \Lambda + \sum_n I_n - n\Phi - \frac{(ne)^2}{4Z_c} - neFZ_c - \Gamma + \frac{1}{2} (\alpha_a - \alpha_i) F^2, \quad (3.3)$$

where Γ is the half-width of the ionic level broadened by its interaction with the atomic curve. A confrontation of these models with experimental data has been presented by Kellogg³², while Forbes^{2,49} has presented several critical assessments.

An early microscopic calculation of $Q(F)$ by Kahn and Ying¹⁴, based on the local density approximation of density-functional theory, treated the metal as a jellium. Kingham¹⁵ has presented some preliminary results, obtained within a tight-binding cluster model, for the field evaporation of Rh. The microscopic theory of field evaporation presented by Kreuzer and Nath²⁰ calculates the electronic properties of the metal within a tight-binding cluster approach based on the ASED-MO method¹⁹, while local electric fields are taken from self-consistent jellium calculations^{10,11}. They extract the activation energy $Q(F)$ from adiabatic ground-state energy curves, and find a scaling law, which predicts evaporation field strengths within 10-20% of experimental values.

To extend such ground-state energy calculations to a kinetic theory of field desorption and evaporation, we have employed a master equation to calculate the energy-dependent ion yield in the thermal field-desorption of helium as a function of field strength and temperature, as presented in Part II. In this part, we will use it to study the field evaporation of metals and present numerical data for field evaporation of W. To summarize our results, we find, as Kreuzer and Nath found in their earlier study²⁰, that: the activation barrier against field strength decreases (monotonically for most metals, such as tungsten, for which we obtain good agreement with Kellogg's data³²), whereas the prefactor initially increases with increasing field strength (up to $4.5V/\text{\AA}$ for tungsten) due to an enhanced ionization probability, and then decreases due to changes in the surface potential of the

desorbing atom.

2. Method

2.1 Adiabatic and Diabatic States

Field evaporation occurs predominantly at kink and step sites, where the electric fields are enhanced. In our theory, we consider a situation, in which a single metal atom sits a distance R away from the topmost ion core on top of an otherwise perfect crystal plane. In Part II, we presented a detailed description of the theory of diabatic and adiabatic states, a brief result of which is cited as following. The total wavefunction of the Hamiltonian of the adatom-metal surface system,

$$H_d = T(R) + H_e(r;R), \quad (3.4)$$

can be expressed as

$$\begin{aligned} \Psi_\alpha(r;R) &= \sum_i \zeta_i(r;R) \chi_{i\alpha}(R) \\ &= \sum_i \zeta_i(r;R) A_{ij}(R) \eta_{j\alpha}(R) \\ &= \sum_j \xi_j(r;R) \eta_{j\alpha}(R), \end{aligned} \quad (3.5)$$

where the adiabatic many-electron wavefunction ζ_i is the eigen-

state of the Hamiltonian of the electron, H_e , with the eigenvalue V_i ,

$$H_e(r;R) \zeta_i(r;R) = V_i(R) \zeta_i(r;R), \quad (3.6)$$

and, if the unitary transition matrix A is subjected to the condition,

$$\left[\frac{\partial}{\partial R} + T^{(1)} \right] A = 0, \quad (3.7)$$

where the operator $T^{(1)}$ is defined as

$$T_{ij}^{(1)}(R) = \int \zeta_i^*(r;R) \frac{\partial}{\partial R} \zeta_j(r;R) dr, \quad (3.8)$$

then the diabatic states of the adatom, η , subject to the equation,

$$\left[-\frac{\hbar^2}{2M} I \frac{\partial^2}{\partial R^2} + W(R) - E \right] \eta = 0, \quad (3.9)$$

with the (coupled) interaction matrix W defined as

$$W = A^\dagger V A. \quad (3.10)$$

In the case of field adsorption of a helium atom on a tungsten surface, the interaction between the adatom and surface is very weak, so that, if the metal surface is approximated with a cluster

model, usually only two levels, one from the adatom and another from the metal, significantly participate in combining orbitals of the adatom-metal system. Therefore, it is possible to only consider two levels (see Fig.2.1), ϕ_a , the highest occupied level in the isolated adatom with the energy ϵ_a , and ϕ_m , the lowest unoccupied level above the Fermi energy of the isolated metal of the same symmetry as ϕ_a with the energy ϵ_m ; while all other electron levels remain unchanged as spectators. These two levels combine into two orbitals, Φ_g and Φ_e , and one can assign the adiabatic many-electron wavefunctions thus that the adiabatic ground-state wavefunction for N electrons,

$$\zeta_0(r;R) = |\Phi_1 \Phi_2 \dots \Phi_{N-1} \Phi_g|, \quad (3.11)$$

is composed of the spectator states, Φ_i for $i=1, \dots, N-1$, and Φ_g , whereas the lowest-excited many-electron wavefunction,

$$\zeta_1(r;R) = |\Phi_1 \Phi_2 \dots \Phi_{N-1} \Phi_e|, \quad (3.12)$$

has Φ_g replaced by Φ_e .

2.2 Perturbative Approach

In the thermal field-evaporation of metal ions, since the adatom and metal surface atoms are identical, the interaction between them is correspondingly very strong. Hence, many levels participate to form molecular orbitals for the adatom-metal

system; this contrasts with the weakly interacting *He* adatom-*W* surface field-desorption case considered in Part II, where it was assumed that only two states participated in molecular orbital formation. As a consequence, many states become important, corresponding to different ionization stages and, more fundamentally, outgoing momentum. In principle, we can use the formalism of adiabatic and diabatic states derived in Part II, but this would require the construction of a large unitary transformation matrices A . In practice, these adiabatic many-electron wavefunctions are very difficult to obtain, as most of them are excited states. Instead, we will advance a perturbative approach to the construction of the diabatic many-electron wavefunctions, ξ , introduced in Eq.(3.5). We observe that an electron is transferred from the adatom to the metal when the highest occupied level on the adatom rises above the Fermi level of the metal. We can linearize the energy of the highest occupied level of the adatom as

$$\epsilon_a(Z) = \epsilon_m + \Delta\epsilon(Z), \quad (3.13)$$

with $\Delta\epsilon(Z_c) = 0$, where Z_c denotes the adatom position when the electron is transferred. Further more, if we restrict ourselves to two levels for the moment, we then write for the orbitals

$$\Phi_g = c_{gm} \phi_m + c_{ga} \phi_a \quad (3.14)$$

and

$$\Phi_e = c_{em} \phi_m + c_{ea} \phi_a . \quad (3.15)$$

Hence we get to second order

$$c_{gm} = \frac{1}{\sqrt{2}} \frac{1-(f-g)S}{\sqrt{1+f^2-fg}} , \quad (3.16a)$$

$$c_{ga} = \frac{1}{\sqrt{2}} \frac{f-g}{\sqrt{1+f^2-fg}} , \quad (3.16b)$$

$$c_{em} = \frac{1}{\sqrt{2}} \frac{1-(f+g)S}{\sqrt{1+f^2+g}} \quad (3.16c)$$

and

$$c_{gm} = \frac{1}{\sqrt{2}} \frac{f+g}{\sqrt{1+f^2+g}} , \quad (3.16d)$$

where

$$f(Z) = \frac{\Delta\epsilon(Z)}{2(V-\epsilon_m S)} , \quad (3.17)$$

$$g = \sqrt{1+f^2} , \quad (3.18)$$

$$V = \langle \phi_m | h | \phi_a \rangle , \quad (3.19)$$

$$S = \langle \phi_m | \phi_a \rangle , \quad (3.20)$$

with h being the single electron Hamiltonian. Thus, the adiabatic many electron wavefunctions, ζ_0 and ζ_1 , are obtained according to

(3.11) and (3.12). The transformation angle, (Eq.(2.25))

$$\theta(Z) = \int_{\infty}^Z dZ \int dr \Phi_g(r;Z) \frac{\partial}{\partial Z} \Phi_e(r;Z), \quad (3.21)$$

is then, with Eqs.(3.11), (3.12), (3.13)-(3.16), given by

$$\theta(Z) = \frac{1}{2} \ln g^{-1} f(Z) - \frac{\pi}{4}. \quad (3.22)$$

Having $\theta(Z)$, we obtain

$$\sin\theta(Z) = -\sqrt{1-f/g} \quad (3.23)$$

and

$$\cos\theta(Z) = \sqrt{1+f/g}. \quad (3.24)$$

We next calculate the diabatic potentials, W_{ij} , from (2.22)-(2.24). First, we note that the total energy V_i of the many-electron wavefunction ζ_i (Eq.(2.5)) is represented in the ASED-MO method as sum of a repulsive term, E_r , and a remainder, E_{npr} : E_r accounts for the Coulomb interaction between isolated atoms and, thus, is determined by the geometry, while E_{npr} entails the (non-perfectly following) electron rearrangement, induced by the presence of the other atoms, and is equal to the sum of the single-electron energies. The difference, $V_0 - V_1$, is related to the difference, $\epsilon_g - \epsilon_e$,

between the terms, E_{npf} , of the many-electron wavefunctions, ζ_0 and ζ_1 . From Eqs.(3.14)-(3.16), we have

$$V_0 - V_1 = -g(V - \epsilon_m S). \quad (3.25)$$

With Eqs.(3.23)-(3.25), we derive for the interaction term, W_{01} , of Eq.(2.24) in a two-state system

$$W_{01}(Z) = V(Z) - \epsilon_m S(Z). \quad (3.26)$$

The diabatic many-electron wavefunctions are then given by

$$\begin{aligned} \xi_0(r;R) &= \cos\theta \zeta_0 - \sin\theta \zeta_1 \\ &= (c_{gm} \cos\theta - c_{em} \sin\theta) |\Phi_1 \Phi_2 \dots \Phi_{N-1} \phi_m| \\ &\quad + (c_{ga} \cos\theta - c_{ea} \sin\theta) |\Phi_1 \Phi_2 \dots \Phi_{N-1} \phi_a| \end{aligned} \quad (3.27)$$

and

$$\begin{aligned} \xi_1(r;R) &= \sin\theta \zeta_0 + \cos\theta \zeta_1 \\ &= (c_{gm} \sin\theta + c_{em} \cos\theta) |\Phi_1 \Phi_2 \dots \Phi_{N-1} \phi_m| \\ &\quad + (c_{ga} \sin\theta + c_{ea} \cos\theta) |\Phi_1 \Phi_2 \dots \Phi_{N-1} \phi_a|. \end{aligned} \quad (3.28)$$

With (3.23) and (3.24), (3.27) and (3.28) reduce when properly normalized to

$$\xi_0(r;R) = (1 - S^2)^{-1/2} (|\Phi_1 \Phi_2 \dots \Phi_{N-1} \phi_a| - S |\Phi_1 \Phi_2 \dots \Phi_{N-1} \phi_m|) \quad (3.29)$$

and

$$\xi_1(r;R) = |\Phi_1 \Phi_2 \dots \Phi_{N-1} \phi_m|, \quad (3.30)$$

where S is the overlap of the levels ϕ_a and ϕ_m , as given in (3.20).

To assess this perturbative approach, we have recalculated a few numbers relevant in the field desorption of helium from tungsten. E.g., in a field of $5.5V/\text{\AA}$, $W_{01}(Z_c) = 1.96\text{meV}$ using the exact transformation, and 1.78meV employing the approximate formula (3.26). In the relevant interval of Z around Z_c , the error is never larger than 30%.

We now want to generalize the perturbative approach to situations where several, or many, levels on the adatom and in the metal participate in the ionization process. With Eq.(3.6), we first rewrite (3.10), the interaction matrix of the Hamiltonian, as

$$W(R) = \int dr A^\dagger \zeta(r;R) H_e \zeta^\dagger(r;R) A. \quad (3.31)$$

Using (3.5), we eventually write the interaction matrix in the diabatic basis as

$$W(R) = \int dr \xi(r;R) H_e(r;R) \xi^T(r;R). \quad (3.32)$$

Assume again that the many-electron wavefunctions can be approx-

imated by single Slater determinants. We denote by ϕ_a the wavefunction of the highest occupied level on the isolated atom and by $\phi_{m,k}$, with $k=1,2,\dots$, single-electron wavefunctions of energy $\epsilon_{m,k}$ above the Fermi level of the isolated metal. To ensure orthogonality, we define

$$|\tilde{\phi}_a\rangle = N_a P_m |\phi_a\rangle, \quad (3.33)$$

where the projection operator is given by

$$P_m = 1 - \sum_k |\phi_{m,k}\rangle\langle\phi_{m,k}|, \quad (3.34)$$

such that the normalization constant becomes

$$N_a^{-2} = 1 - \sum_k \langle\phi_{m,k}|\phi_a\rangle^2. \quad (3.35)$$

The lowest energy diabatic many-electron wavefunction with both adatom and metal neutral, then, is given by

$$\xi_0(r;R) = \left| \Phi_1 \Phi_2 \dots \Phi_{N-1} \tilde{\phi}_a \right|. \quad (3.36)$$

The excited wavefunctions,

$$\xi_k(r;R) = \left| \Phi_1 \Phi_2 \dots \Phi_{N-1} \phi_{m,k} \right|, \quad (3.37)$$

describe the situation in which one electron has been transferred from the adatom to the k th level above the Fermi energy of the metal. Writing the electronic Hamiltonian as a sum of single-electron contributions,

$$H_e(r;R) = \sum_{i=1}^N h(r_i;R), \quad (3.38)$$

and inserting (3.36) and (3.37) into (3.32), we get for the off-diagonal terms

$$W_{0k}(R) = N_a (V_k - \epsilon_{m,k} S_k), \quad (3.39)$$

where

$$V_k = \langle \phi_a | h | \phi_{m,k} \rangle \quad (3.40)$$

is the interaction between levels ϕ_a and $\phi_{m,k}$, and

$$S_k = \langle \phi_a | \phi_{m,k} \rangle \quad (3.41)$$

is the overlap between them. This completes the perturbative approach to the calculation of the diabatic interaction matrix (3.32).

3. Results

In Part II of this thesis, we outlined the derivation of the kinetic equations that control field ionization, field desorption and field evaporation, and, in particular, we derived an expression for the yield of singly charged ions

$$Y_{ion} = \frac{\sum_{\nu, k_+} T_{+0}(k_+, \nu) \exp(-E_{0\nu} / k_B T)}{\sum_{\nu} \exp(-E_{0\nu} / k_B T)}, \quad (3.42)$$

where

$$T_{ij}(\nu, \mu) = \frac{2\pi}{\hbar} \left| \int d\mathbf{R} \eta_{i\nu}^*(\mathbf{R}) W_{ij}(\mathbf{R}) \eta_{j\mu}(\mathbf{R}) \right|^2 \Delta(E_{i\nu} - E_{j\mu}, \Gamma_{j\mu}) \quad (3.43)$$

with

$$\Delta(\epsilon, \Gamma) = \frac{1}{\pi} \frac{\Gamma/2}{\epsilon^2 + \Gamma^2/4}. \quad (3.44)$$

Here $\Gamma_{j\mu}$ is the half-width of the level μ in the diabatic potential W_{jj} due to phonon transitions. Because $T_{ij}(\nu, \mu)$ describes transitions between discrete states of the unperturbed Hamiltonian, care must be exercised to include the width of the initial state. This is done formally by replacing the energy conserving δ -function by the Lorentzian (3.44).

We will now report numerical results for the thermal field-evaporation of tungsten ions from a tungsten tip. We model the tungsten tip by a finite-sized cluster of tungsten atoms, which, to mimick an isolated atom on a (111) surface, is chosen as three atoms in a plane, with an additional atom below the midpoint of the triangle, and a fifth one in the symmetrical position above the plane. Our calculations are based on the semi-empirical ASED-MO method, described in Ref.20; parameters used for W are those of Ref.20, except that we have raised, in an ad hoc manner, the ionization energies for the adatom by 1.5eV so that we can describe by one set of parameters both the neutral and ionic states of this atom. In this approach, we unfortunately cannot incorporate the electric field in a self-consistent manner. However, because the local variation of the electric field is important, we take the electric field from self-consistent density-functional calculations^{10,11} for a plane jellium metal and assign a Wigner-Seitz radius $r_s=2.07$ to tungsten. We then impose this field onto the cluster, assuming that the jellium edge is half a lattice spacing above the plane of atoms in our cluster.

To determine the transition probabilities (3.43), we must know the nuclear wavefunctions, $\eta_{0\nu}^0$ and $\eta_{+\mu}^0$, in the diabatic potentials, W_{00} and W_{++} . To simplify the numerics, as done in Part II, we have fitted a Morse potential to W_{00} , i.e.,

$$W_{00}(Z) = A_0(F) [\exp[-2\gamma(Z-Z_0)] - 2\exp[-\gamma(Z-Z_0)]] , \quad (3.45)$$

adjusting its parameters, $A_0(F)$, $\gamma(F)$ and $z_0(F)$, as a function of field strength, and, likewise, we set

$$W_{++}(Z) = W_c - eF(Z - Z_c) \quad (3.46)$$

for W_{++} , the diabatic potential energy curve of the ion. For both potentials, the wavefunctions can be given analytically.

Field evaporation being an activated process, it is instructive to parametrize the ion yield rate constant according to the Polanyi-Wigner equation (3.1). In Table 3.1, we present the relevant data. We note first that the activation energies for field evaporation, $Q(F)$, agree well with experiment. To put this into perspective, we point out that this agreement depends on our choice for r_s , as discussed in Ref.20, e.g., if we take $r_s=1.5$, the calculated evaporation field strength increases to $8V/\text{\AA}$ from its value of $6V/\text{\AA}$ at $r_s=2.07$.

Turning next to the prefactor $\alpha\nu$, we first note its dependence on field strength. In the early days of field ion spectroscopy, it had been assumed that the prefactor was independent of field strength.⁵⁴ However, Kellogg³² has found a substantial field dependence in the field evaporation of tungsten. For the thermal field-desorption of helium, such a field dependence results from changes in the shape of the surface potential in which helium is adsorbed, as explained in Part II. For field evaporation, this effect is also present, albeit of lesser significance. To obtain a

Table 3.1: Field dependence of the activation barrier, Q , and the prefactor, av , experimental data from Ref.32 and also the ground state frequency ν_0 and the excited frequency ν_1 for $h\nu_1=Q$ (for details see text)

Field (V/Å)	Q (eV)		k_0 (s ⁻¹)		ν_0 (s ⁻¹)	n_1	$\nu_1 = (2n_1 + 1)\nu_0$ (s ⁻¹)
	Exp.	Calc.	Exp.	Calc.			
3.0	-	1.85	-	1.01×10^{14}	2.92×10^{12}	99	4.58×10^{14}
3.50	-	1.72	-	1.83×10^{14}	4.93×10^{12}	55	5.47×10^{14}
4.0	-	1.42	-	2.33×10^{14}	4.55×10^{12}	49	4.54×10^{14}
4.5	-	1.22	-	2.93×10^{14}	4.62×10^{12}	41	3.78×10^{14}
4.70	0.90	1.17	3×10^{16}	2.76×10^{14}	4.52×10^{12}	37	2.86×10^{14}
4.93	0.60	0.85	1×10^{13}	2.60×10^{14}	4.00×10^{12}	30	2.11×10^{14}
5.10	0.52	0.58	8×10^{12}	2.21×10^{14}	3.51×10^{12}	24	1.58×10^{14}
5.30	0.35	0.41	7×10^{11}	2.25×10^{14}	3.17×10^{12}	18	1.10×10^{14}
5.47	0.31	0.31	7×10^{11}	2.06×10^{14}	2.83×10^{12}	15	8.30×10^{13}
5.72	0.20	0.20	3×10^{11}	1.66×10^{14}	2.68×10^{12}	10	5.37×10^{13}
5.92	0.12	0.12	4×10^{11}	5.46×10^{13}	2.64×10^{12}	7	3.82×10^{13}

better understanding, we recall that in field-free thermal desorption, the desorption rate constant at low coverage can be written, for desorption from a mobile, nonlocalized adsorbate, as

$$r_d = S\nu_z \exp(-E_d/k_B T) \quad (3.47)$$

when $h\nu_z \ll k_B T$, and as

$$r_d = S \frac{k_B T}{h} \exp(-E_d/k_B T) \quad (3.48)$$

when $h\nu_z \gg k_B T$. For desorption from a localized adsorbate, we get

$$r_d = S \frac{2\sqrt{Ma_s}}{k_B T} \nu_x \nu_y \nu_z \exp(-E_d/k_B T), \quad (3.49)$$

where ν_x , ν_y and ν_z are the vibrational frequencies of the adsorbed particle at the bottom of the surface potential well in the x , y , and z directions. Note that to ensure detailed balance, the desorption rate also contains the sticking coefficient S , which is a measure of the efficiency of energy transfer between the solid and the adatom.

In field desorption and field evaporation, the adatom must be thermally excited up to the energy of the potential barrier; this is a process akin to thermal desorption. Subsequently, it must get ionized. Thus the prefactor consists of two factors, namely an ionization probability $\alpha(F)$ and an attempt frequency $\nu(F)$.

Their field dependences are opposing each other in that $\alpha(F)$ increases from zero in zero field to one at "high" fields, whereas $\nu(F)$ decreases. We can view this process as a particle localized in the excited level, $\epsilon_i \approx Q(F)$, at the energy of the potential barrier attempting with a frequency $\nu_i = \epsilon_i/h$ of that level to ionize with a probability $\alpha(F)$. Because $Q(F)$ decreases with F , so does ϵ_i and thus ν_i . In addition, the hump of the activation barrier and thus the region for ionization moves towards the metal for increasing field, resulting in an increasing ionization probability $\alpha(F)$. In Table 3.1, we have estimated the critical energy level in W_{00} , assumed to be a Morse potential, and find that, e.g., for $F=4.7 V/\overset{0}{\text{Å}}$, the adatom is in the 37th excited state when it attempts to ionize. This level has a frequency $\nu_{37}=2.86 \times 10^{14} \text{s}^{-1}$ as opposed to the ground state frequency $\nu_0=4.5 \times 10^{12} \text{s}^{-1}$. This compares rather well with the prefactor of $2.76 \times 10^{14} \text{s}^{-1}$ obtained from the Polanyi-Wigner parametrization of the ion yield. This argument should, however, not be taken too literally as other factors contribute to the prefactor, as one already knows from the simpler situation of thermal desorption, cf. equations (3.47)-(3.49). We can guess that, for fields less than $4.5 V/\overset{0}{\text{Å}}$, the field dependence of $\alpha(F)$ dominates, and most likely $\alpha(F)=1$ for larger fields, and, for fields stronger than $4.5 V/\overset{0}{\text{Å}}$, the decrease in $\nu(F)$ becomes dominant.

Although our theory produces the right trend in the prefactor, namely decreasing with increasing field for fields larger than $4.5 V/\overset{0}{\text{Å}}$, as observed by Kellogg, there are discrepancies in the absolute values in that the experimental data are substantially

lower except at $F=4.7V/\text{\AA}$. However, Kellogg warns that his prefactors have an uncertainty of at least one order of magnitude. On the other hand, our theoretical values may also be out by an order of magnitude due to several of our approximations, in particular, neglecting lateral variations in the electric field, which might effect the localization of the adatom. Also, recall that the master equation, that underlies (3.42) as derived in Refs.7,45, is restricted in its applicability to the Markovian limit. With prefactors of the same order ($10^{14}s^{-1}$) as thermal phonon-assisted transitions in W_{00} , one should account for non-Markovian effects by, e.g., using the Tsukada-Gortel equations⁵⁰, which will result in lower prefactors, but most likely not more than one order of magnitude.

We would like to comment further on the difference in prefactors for the field evaporation of tungsten and the thermal field-desorption of helium. For the latter case, we found prefactors increasing more or less exponentially from a low of 10^6s^{-1} at $F=4V/\text{\AA}$ to a high of $10^{12}s^{-1}$ at $6V/\text{\AA}$, as shown in Fig.2.4. This has been interpreted as due to an increase in the ionization probability $\alpha(F)$ due to rapidly increasing overlap of wave functions on the helium and in the metal. At similar field strengths, the activation barrier for helium increases substantially, whereas, for metal field-evaporation, the activation barrier decreases monotonically. For helium the field enhances adsorption, at least up to $6V/\text{\AA}$ ^{18,24}, although this enhancement ceases, most likely around $7V/\text{\AA}$, due to the same effects as that causes a monotonic weakening

of the surface bond for metals on metals, namely a draining of the electron charge on bonding orbitals into the metal.

We have thus far presented results on thermal field-evaporation of singly charged tungsten ions, while experiment only detects W^{3+} and W^{4+} ions. The fact that our calculated prefactors are rather large, i.e., of the order of $10^{14}s^{-1}$, we take as evidence to suggest that the first ionization stage from W to W^+ must be the slowest, i.e., rate determining step. Because the tunneling rate into the metal decreases rapidly with increasing distance, the higher ionization states cannot be produced by tunneling into the metal, as their abundance would in that case be decreased over singly charged ions roughly by the ratio of the ionization rates. Thus post-ionization^{53,55} occurs at least several angstroms away from the surface, but still in the high-field region, with the excess electrons tunneling into vacuum states rather than empty metal states. Simple-minded estimates confirm this scenario, although detailed calculations, e.g., for tungsten, are not available at this stage.

4. Conclusions

In this part of the thesis, we have applied the recent theory of the kinetics of field ionization, field desorption and field evaporation to study the field evaporation of tungsten. We have developed a perturbative method to calculate diabatic states from adiabatic ones. We find good agreement of the field dependence of

the calculated activation barrier with experimental data. We also find that the prefactor in the ion yield increases initially, up to the field strength of about $4.5V/\text{\AA}^0$ for tungsten, due to a rapid increase in the ionization probability and then decreases with increasing field strength due to changes in the surface potential. There is some discrepancy in the absolute value, which must be resolved by better experiments and by a better theory, for example, for the latter, a theory based on the spin density functional theory to more properly account for charged species by a better treatment of Coulomb effects.

*The former name of the author was Liang-Chen Wang (L.C. Wang).

References

1. H.J. Kreuzer, in *Chemistry and Physics of Solid Surfaces VIII*, eds. R. Vanselow and R. Howe (Springer-Verlag, Berlin, 1990).
2. R.G. Forbes, *J. Phys.* D18 (1986) 973.
3. N. Ernst and G. Ehrlich, in *Microscopic Methods in Metals*, Vol.40 of *Topics in Current Physics*, ed. U. Gonser (Springer-Verlag, Berlin, 1986).
4. J.H. Block, in *Chemistry and Physics of Solid Surfaces IV*, eds. R. Vanselow and R. Howe (Springer-Verlag, Berlin, 1982).
5. H.J. Kreuzer, L.C. Wang and N.D. Lang, *Phys. Rev. B* (in press).
6. H.J. Kreuzer and L.C. Wang, *J. de Physique*, 50 (1989) C8-9.
7. H.J. Kreuzer, K. Watanabe, and L.C. Wang, *Surface Sci.* 232 (1990) 379.
8. L.C. Wang and H.J. Kreuzer, *Surface Sci.* 237 (1990) 337.
9. N.D. Lang and W. Kohn, *Phys. Rev.* B1 (1970) 4555; B3 (1971) 1215; B7 (1973) 3541.
10. P. Gies and R.R. Gerhardt, *Phys. Rev.* B33 (1986) 982.
11. F. Schreier and F. Rebentrost, *J. Phys.* C20 (1987) 2609.
12. J.E. Inglesfield, *Surf. Sci.* 188 (1987) L701.
13. G.C. Aers and J.E. Inglesfield, *Surface Sci.* 217 (1989) 367.
14. L.M. Kahn and S.C. Ying, *Solid State Commun.* 16 (1975) 799; *Surf. Sci.* 59 (1976) 333.
15. D.R. Kingham, in *Proceedings of the 29th International Field Emission Symposium*, eds. H.O. Andren and H. Norden (Almqvist and Wiksell, Stockholm, 1983).

16. D. Tomanek, H.J. Kreuzer and J.H. Block, *Surf. Sci.* **157** (1985) L315.
17. K. Nath, H.J. Kreuzer and A.B. Anderson, *Surf. Sci.* **176** (1986) 261.
18. N. Ernst, W. Drachsel, Y. Li, J.H. Block and H.J. Kreuzer, *Phys. Rev. Lett.* **57** (1986) 2686.
19. A.B. Anderson and R.G. Parr, *J. Chem. Phys.* **53** (1970) 3375; A.B. Anderson, *J. Chem. Phys.* **60** (1974) 2477; **62** (1975) 1187; **63** (1975) 4430.
20. H.J. Kreuzer and K. Nath, *Surf. Sci.* **183** (1987) 591.
21. E.W. Müller, S.B. MacLane and J.A. Panitz, *Surf. Sci.* **17** (1969) 430.
22. E.W. Müller and Ber. Bunsenges, *Phys. Chem.* **75** (1971) 979.
23. T.T. Tsong and E.W. Müller, *J. Chem. Phys.* **55** (1971) 2884.
24. N. Ernst, *Surf. Sci.* **219** (1989) 1.
25. T.T. Tsong and E.W. Müller, *Phys. Rev. Lett.* **25** (1970) 911.
26. K. Watanabe, S.H. Payne and H.J. Kreuzer, *Surf. Sci.* **202** (1988) 521.
27. N.D. Lang, in *Solid State Physics*, ed. by F. Seitz, D. Turnbull and H. Ehrenreich (Academic Press, New York, 1973), vol.28, p.225.
28. N.D. Lang and A.R. Williams, *Phys. Rev.* **B18** (1978) 616.
29. W. Kohn and L.J. Sham, *Phys. Rev.* **140** (1965) A1133.
30. L. Hedin and B.I. Lundqvist, *J. Phys.* **C4** (1971) 2064.
31. T.T. Tsong, *Surface Sci.* **70** (1978) 211.
32. G.L. Kellogg, *Phys. Rev.* **B29** (1984) 4304.
33. D.J. Rose, *J. Appl. Phys.* **27** (1956) 215.

34. G.L. Kellogg and T.T. Tsong, *Surface Sci.* 62 (1977) 343.
35. H.J. Kreuzer and Z.W. Gortel, *Physisorption Kinetics*, Springer Series in Surface Sciences, vol.1 (Springer-Verlag, Berlin, 1986).
36. N.D. Lang and J.K. Norskov, *Phys. Rev.* B27 (1983) 4612.
37. N.D. Lang, *Phys. Rev. Lett.* 46 (1981) 842.
38. P.W. Anderson, *Phys. Rev.* 124 (1961) 41.
39. D.M. Newns, *Phys. Rev.* 178 (1969) 1123.
40. E.W. Müller and T.T. Tsong, *Field-Ion Microscopy, Principles and Applications* (Elsevier, Amsterdam, 1969).
41. E.W. Müller and T.T. Tsong, *Prog. Surface Sci.* 4 (1973) 1.
42. E.W. Müller, *Naturwissenschaften* 29 (1941) 533.
43. E.W. Müller, *Phys. Rev.* 102 (1956) 618.
44. S.H. Payne and H.J. Kreuzer, *Surf. Sci.* 205 (1988) 153.
45. H.J. Kreuzer and K. Watanabe, *J. de Physique* 49 (1988) C6-7.
46. This condition can not, in general, be satisfied, as shown by C.A. Mead and D.G. Truhlar, *J. Chem. Phys.* 77 (1983) 6090. However, there is no difficulty in our problem. For further discussions of this point, see, e.g., H. Köppel, W. Domke, and L.S. Cederbaum, *Adv. Chem. Phys.* 57 (1985) 59.
47. R. Gomer, *J. Chem. Phys.* 31 (1959) 341.
48. R. Gomer and L.W. Swanson, *J. Chem. Phys.* 38 (1963) 1613.
49. R.G. Forbes, *Surf. Sci.* 102 (1982) 255.
50. M. Tsukada and Z.W. Gortel, *Phys. Rev.* B38 (1989) 3892.
51. T.T. Tsong, *Surf. Sci.* 177 (1986) 593.
52. E.W. Müller, *Phys. Rev.* 102 (1960) 618.
53. N. Ernst, *Surface Sci.* 87 (1979) 469.

54. T.T. Tsong, J. Chem. Phys. 54 (1971) 4205.
55. R. Haydock and D.R. Kingham, Phys. Rev. Lett. 44 (1980) 1520;
Surf. Sci. 104 (1982) L194.